# Validating mechanistic models of fluid displacement during imbibition

*Sharon Ellman[1,2] – email address: sharon.ellman@ugent.be*
*Arjen Mascini[1,2] – email address: arjen.mascini@ugent.be*
*Tom Bultreys[1,2]– email address: tom.bultreys@ugent.be*

*[1]PProGRess,Dept. of Geology, Ghent University, Krijgslaan 281/ S8, 9000 Ghent, Belgium*
*[2]Centre for X-ray Tomography, Ghent University, Proeftuinstraat 86, 9000 Ghent, Belgium*

This paper is a non-peer reviewed preprint submitted to EarthArXiv.

Corresponding author: Sharon Ellman, sharon.ellman@ugent.be

# Validating mechanistic models of fluid displacement during imbibition

*Sharon Ellman[a,b,*], Arjen Mascini[a,b] and Tom Bultreys[a,b]*

*[a]PProGRess,Dept. of Geology, Ghent University, Krijgslaan 281/ S8, 9000 Ghent, Belgium*

*[b]Centre for X-ray Tomography, Ghent University, Proeftuinstraat 86, 9000 Ghent, Belgium*

** Corresponding Author. Address: Krijgslaan 281/S8, 9000 Ghent, Belgium*

*E-mail address: Sharon Ellman (Sharon.ellman@UGent.be).*

*Keywords:*

Capillary pressure

Pore network models

Multiphase flow

X-ray imaging

*Abstract:*

Pore-scale modelling is an important tool to improve our understanding of multiphase flow in porous media. Slow fluid invasion is commonly modelled using quasi-static pore network models (PNM). These models simulate the invasion in a network of simplified pores and throats by invading network elements in order of the quasi-static "invasion" capillary pressure needed for the invading fluid to enter. Despite a multitude of studies that address the predictiveness of PNM, it remains unclear what the leading causes of errors in these methods are, particularly during imbibition. To address this, we developed a novel method to directly validate the invasion capillary pressure models that underlie quasi-static PNM for the first time. The new method compares these models to local capillary pressures measured during in-situ flow experiments visualized with 4D µCT. We applied this to two different open-source PNM extractions from a µCT dataset of a glass beads pack that underwent slow imbibition. This methodology is limited by the temporal resolution of the data, hence we tested assumptions regarding displacement sequences when individual displacements could not be resolved. To constrain the uncertainty on the input parameters, we used local contact angles measured from the µCT images. In the PNMs we investigated, the model-predicted invasion-Pc values were on average greater than the direct measurements made using curvatures from the µCT images. Important sources of mismatch were the difficulty to accurately describe the pore space of a beadpack as a network of pores and throats, as well as the relatively low temporal resolution of the µCT dataset. The method presented here can be used to direct the development of improved pore network models.

## I. INTRODUCTION

Multiphase flow in permeable materials is of vital importance to several issues facing the world at present. It is key to several geo-engineering challenges, such as contaminant transport and subsequent remediation [1,2], subsurface energy storage [3] and carbon dioxide sequestration [4,5]. Field-scale models attempt to predict fluid flows at the application scale. These large-scale models require constitutive properties as input, such as capillary pressure (Pc) and relative permeability curves. These properties are difficult to measure and their dependence on controlling factors (such as interfacial curvatures, contact angles, pore space morphology [6], etc.) is poorly understood [7]. To address these problems,

significant research effort has been devoted to developing models which can predict the constitutive properties needed for field-scale models based on the microscopic, pore-scale properties of porous media samples.

Pore-scale multiphase flow modelling is challenging due to the need to track many complex fluid menisci as they move through the porous medium, giving rise to intricate patterns in how the fluids occupy the pores in the system [8,9]. These fluid occupation patterns play an important role in the constitutive properties needed for large-scale modelling. The need to capture pore-scale fluid arrangements has given rise to the development of a range of different numerical methods, as reviewed in Bultreys et al. [10]. The two main categories are simplified pore networks and models that run directly on the pore space (i.e., direct approaches). These can be further broken up into quasi-static and dynamic approaches [11]. Direct dynamic simulations solve the flow on a grid or mesh that captures the pore walls in as much detail as possible. They are typically based on the Lattice Boltzmann method or Navier-Stokes discretization approaches (e.g. finite volume methods) [12]. Due to their computational constraints, these methods are limited to small spatial and temporal domains, typically below that of fluid clusters, which is the minimum scale needed to perform upscaling [7]. To remedy this, quasi-static models which act directly on the image of the pore space have been explored [13,14]. These are traditionally most suitable for drainage, as they are unable to represent snap-offs during imbibition or lack volume preservation of disconnected ganglia during trapping (with the exception of Jettestuen et al. [15]). In pore network models (PNMs), on the other hand, the pore space is represented as a network of pores connected by throats, both with an idealized geometry [16]. Methods to extract a pore network from images of the pore space have been developed since the 1990s [17,18]. Coarsely speaking, there are four different methods of splitting up the pore space into pores and throats: there is the medial axis approach [17,19], the grain-based approach [18,20], the maximum ball method [21,22] and the watershed segmentation approach [23,24]. The discretization is then followed by calculating geometrical properties of each network element in a variety of ways [10]. Simplified rules governing the transport and arrangement of fluids are applied over the system so that macroscopic properties can be estimated [16]. This method's efficiency means it can be applied over relatively large spatial domains, though this comes at the cost of a reduced predictive capability and accuracy [12,25]. Because PNMs are simplifications of the process, using them can help us test whether the simplifications in them are reasonable or useful, and therefore improve our mechanistic understanding of multiphase flow. This implies that they may be useful as tools to analyse which aspects of the studied processes require further investigation.

Despite the significant body of research on and with pore-scale models, and specifically quasi-static PNM, in the last 30 years, one of the main outstanding questions is how well they represent real multiphase flow processes [7,26–29]. A key point of interest here is to validate how well these models reproduce fluid displacements. Recent studies have compared fluid distributions predicted by PNMs to pore-scale imaging experiments of drainage and imbibition (the displacement of a wetting fluid by a nonwetting fluid from the pores and vice versa), and mainly found discrepancies for imbibition [7,27]. The causes for these discrepancies have however been difficult to pin down from the fluid distributions alone, as these are only the outcome of the underlying displacement models employed by the PNM. Quasi-static PNMs simulate the filling of the pore space with an invading fluid by taking into account the pressure difference between the two fluids (the "capillary pressure" or "Pc") when the two fluids would be at equilibrium. The model assesses the Pc when different accessible pores would be invaded, and then chooses the option with the most beneficial invasion-Pc (i.e., the pore or throat with invasion-Pc closest to the current equilibrium). During drainage, this results in an incremental invasion from low to high invasion-Pc, while this order is reversed during imbibition [30]. The calculation of the invasion-Pc

Corresponding author: Sharon Ellman, sharon.ellman@ugent.be

values thus controls the predicted sequence in which the invading fluid occupies the pore space, and thereby the fluid distribution patterns that emerge.

In this paper, we address the problem of validating quasi-static PNMs by developing a novel method to directly verify the underlying models that control fluid displacement, rather than only the resulting fluid distributions as performed in previous approaches [7,27]. Validating these invasion-Pc models on a displacement-by-displacement basis has not been done before due to the difficulty of measuring local fluid-fluid curvatures (i.e. capillary pressure) during a fluid displacement experiment [31]. Obtaining local curvatures requires high resolution time-resolved µCT images [6,31] which has only recently become possible [32–35]. Another challenge to perform this validation has been the need to supply accurate fluid-fluid-solid contact angles to the displacement models. In PNM, contact angles have often been approached as tuning parameters to make the model fit measurements of core-scale constitutive properties, rather than as an independently measured microscopic property of the system. The techniques to measure contact angles inside porous media have only recently been developed [31,36–38]. This explains why it was previously only possible to validate PNMs using core-scale measurements [11,16,18] or µCT images of fluid distributions [7,27].

We use the novel invasion-Pc validation method to verify two different PNMs on a µCT dataset of imbibition in a glass beads pack [39] in order to pin down the leading causes of error in these models. To do this, the pore networks were extracted from the glass beads pack dataset and were then used to identify imbibition displacements. Then, instead of assigning advancing contact angles randomly from a range which is assumed reasonable as has been previously done when using PNMs [27,40–42], we measured a local advancing contact angle for each displacement directly from the µCT images. This has the potential to improve the predictive capabilities of PNMs [27,36,43,44]. These provided the inputs needed for the PNMs, which were then used to predict the invasion-Pc for each identified displacement. Next, the fluid menisci were extracted from the experiment to determine curvatures on a displacement-by-displacement basis. To validate the PNMs, we compared the predicted invasion-Pc values to local Pc values determined from the curvatures of the fluid menisci. Below, we first briefly review pore-scale displacements and capillary pressures in Sec. II. Then we describe the experimental data in Sec. III A, followed by an explanation of the methodology used in Sec. III B and C. Next, we discuss the results from the contact angle measurements in Sec. IV A and validation of the image-based curvatures in Sec. IV B. We then discuss the results from the PNM simulation in Sec. IV C and discuss the results from the underlying models compared to the image-based values in Sec. IV D. This is followed by conclusions in Sec. V.

# II. Pore-scale displacements and capillary pressures

## A. Types of displacements

Multiphase flow in the subsurface is typically slow, characterized by capillary numbers below $10^{-7}$, and is hence assumed to be dominated by capillary forces [45]. Fluid flow therefore consists of sequences of discrete fluid displacements [46,47] interspersed with reversible movements such as film growth or menisci curvature changes [48,49]. When nonwetting fluid displaces wetting fluid, it is called drainage. The opposite process of drainage is called imbibition, which is when wetting fluid displaces nonwetting fluid. Imbibition is more complex than drainage as it may, for example, include trapping of nonwetting fluid in the pore space due to pre-existing wetting layers [46]. This work focuses on imbibition.

Imbibition occurs as a combination of piston-like displacements, cooperative pore-fillings and snap-offs [16]. Piston-like displacements occur when the wetting fluid displaces the nonwetting fluid in a pore which is connected to only one throat filled with nonwetting fluid (FIG. 1(a)). This type of displacement

Corresponding author: Sharon Ellman, sharon.ellman@ugent.be

does not change the connectivity of the fluid and is comparable to the Haines jumps [50] which occur during drainage.

A cooperative pore-filling occurs when the wetting fluid displaces the nonwetting fluid in a pore which is connected to two or more surrounding throats filled with nonwetting fluid. In these instances, the radius of curvature of the meniscus is larger than the single pore would dictate, as the interface extends partly into the involved throats (FIG. 1(b)). These events are classified in terms of fluid configurations by the $I_n$ symbol, where 'n' represents the number of surrounding throats filled with nonwetting fluid as the displacement occurs [47].

Snap-off occurs when wetting fluid layers inside of throat corners swell due to the decreasing local Pc, and eventually touch. This forms an unstable interface which rapidly expels nonwetting fluid from the throat, thereby "snapping off" the nonwetting fluid connection between the two neighbouring pores. This alters the connectivity of the nonwetting fluid within the pore space [51] (FIG. 1(c)).

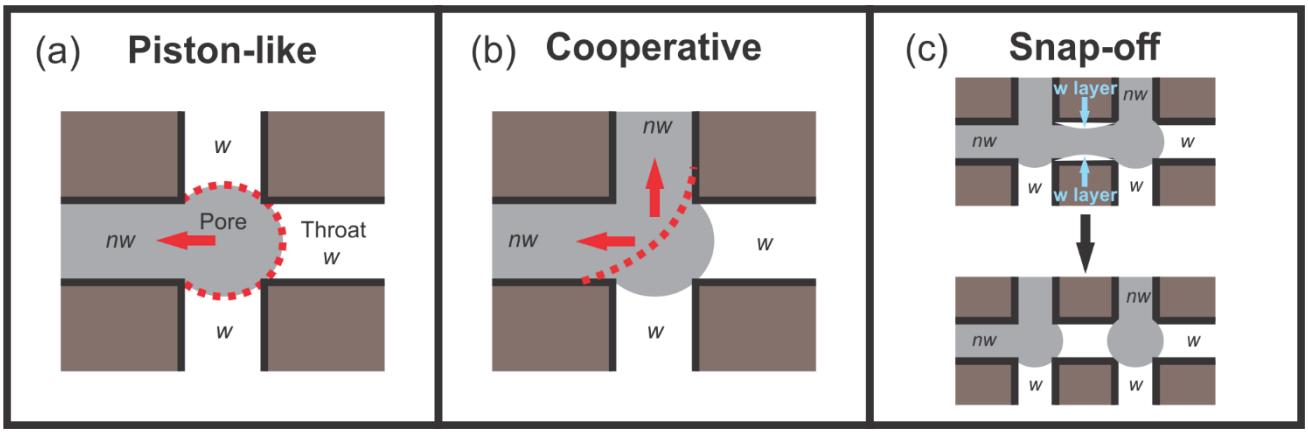


FIG. 1. The dashed red line represents the position of the meniscus immediately prior to the displacement in (a) and immediately after the displacement in (b). (a) Piston-like displacement, (b) Cooperative pore-filling, specifically an $I_2$ displacement as two throats are filled with nonwetting fluid as the displacement occurs, (c) Snap-off. 'w' represents the wetting fluid and 'nw' represents the nonwetting fluid. These diagrams were adapted from Singh et al. [47].

## B. Capillary pressure definitions

Large scale models need constitutive inputs which describe the flow, one of the most important of which is the macroscopic Pc (which we will refer to as $P^c$) [45]. This is the pressure difference between the nonwetting fluid and the wetting fluid measured over the whole sample, and is typically plotted against the average wetting saturation of the porous medium. The $P^c$ is a non-trivial averaging of the local Pc throughout the medium, assuming static conditions and connected phases [52]. The local Pc in turn is the pressure difference across a meniscus at a certain point in the sample and at a given moment in time [45].

When the local Pc is at its equilibrium value, the fluid interface remains stationary. When the local Pc is above or below the equilibrium Pc, the meniscus, by definition, advances or recedes. During imbibition, when the local Pc reaches the lowest equilibrium Pc associated to a pore, (most of) the nonwetting fluid is suddenly evacuated from it [45]. This threshold value is referred to as the invasion-Pc. During capillary dominated flow, the invasion-Pc is therefore assumed to control the sequence in which fluid displacements occur [45].

## C. Invasion percolation

Invasion percolation is an algorithm to approximate how fluids invade the pore space during capillary dominated two-phase flow [53]. For imbibition, at each point during the invasion of the network,

Corresponding author: Sharon Ellman, sharon.ellman@ugent.be

the algorithm first looks for all accessible displacements – meaning the network elements for which the wetting fluid has a connected path to enter and the nonwetting fluid has a path to escape from. The accessible displacement which corresponds to the highest invasion-Pc is then assumed to occur first [53]. This is because the $P^c$ is assumed to slowly decrease during imbibition. The opposite is true for drainage, where displacements corresponding to lower invasion-Pc values are assumed to occur first. These methods assume displacements are infinitely slow and therefore do not consider any influences of viscous or inertial forces that may impact the invasion sequence. In invasion percolation, the sequence in which fluid displacements occur is therefore controlled by the invasion-Pc. Following these rules, we find that smaller pores are invaded first during imbibition and that piston-like displacements and snap-offs are favoured as they occur at higher invasion-Pc values [47].

## D. Invasion-Pc modelling

Different models are required to predict the quasi-static invasion-Pc values at which different types of imbibition displacements are expected to occur. In this work, we used models designed for pore networks of rock samples, as this is our main application area of interest. Specific models for other types of materials (e.g. bead packs [54]) exist, but were not included for this reason. In light of the model choice, it should be noted that in sphere packs the pore and throat locations identified by inscribed spheres only capture the location of the meniscus movement if the contact angle is zero, resulting in possible deviations in the model [55,56]. The employed models are described below.

### *1. Piston-like displacements*

During piston-like displacements, the wetting fluid invading the pore has only one path through which it can advance, hence the Young Laplace equation for cylindrical geometries (1) can be used to calculate the invasion-Pc by assuming the pore is locally cylindrical in shape [31]. $\theta$ is the advancing contact angle measured through the densest phase, $r$ is the pore radius of the invaded pore and $\sigma$ is the interfacial tension.

$$Pc = \frac{2\sigma \cos\theta}{r} \quad (1)$$

### *2. Cooperative pore-fillings*

The geometry-based cooperative pore-filling model developed by Ruspini et al. [57] is the only quasi-static PNM algorithm which takes the local pore structure and fluid topology into account when determining cooperative pore-filling invasion-Pc values. The model accounts for the geometrical characteristics of the pore, the spatial distribution of the throats surrounding the invaded pore as well as the fluid topology at the moment of displacement. It assesses the filling states of the throats surrounding the invaded pore and trigonometrically calculates the curvature of the meniscus in the plane defined by the centrelines of the two throats, which is a 2D approximation. To do this, it uses the given advancing contact angle and the relative position of the throats (FIG. 2). This curvature is then used to calculate the invasion-Pc for that pore. It is assumed that the pair of throats which are filled with nonwetting fluid and have the largest angular spacing govern the invasion-Pc. The equations to calculate the invasion-Pc from this information can be found in the supplementary material [58].

Corresponding author: Sharon Ellman, sharon.ellman@ugent.be

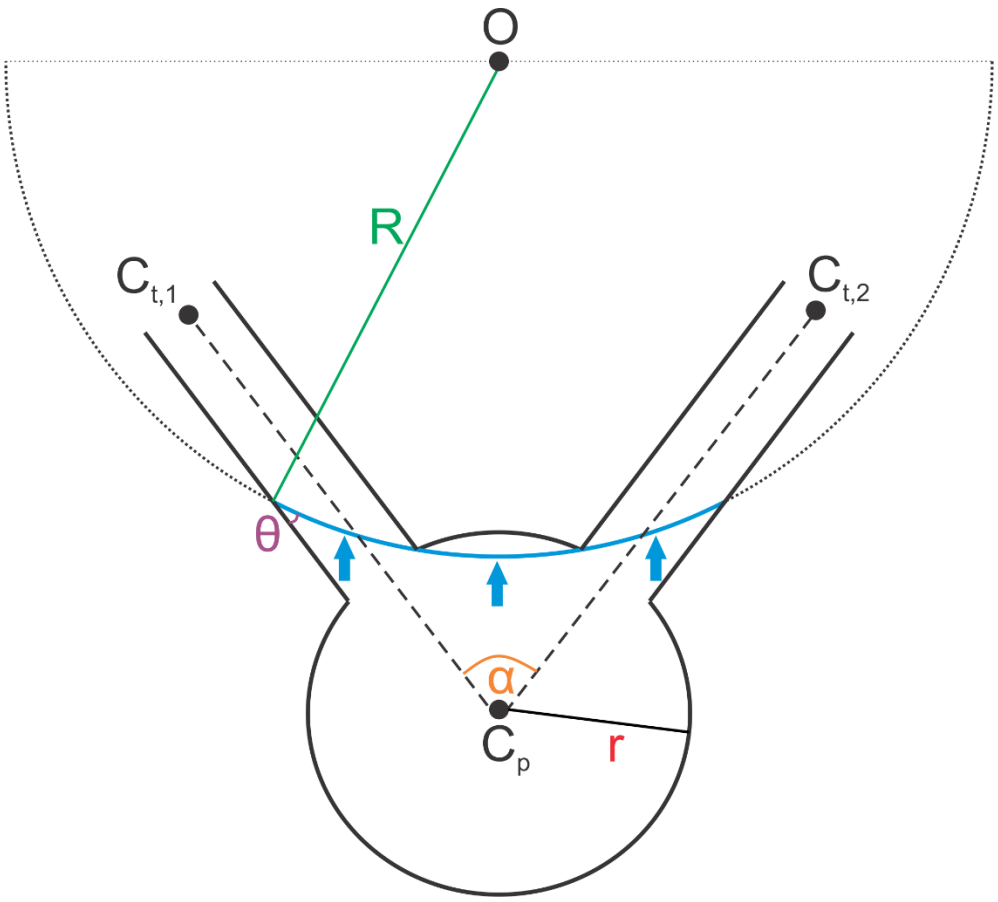


FIG. 2. Geometrical description of an advancing fluid interface used in the cooperative pore-filling model, adapted from [57]. The pore is spherical/cylindrical in shape. The model uses $C_p$ (centre of the pore) and $C_{t,1}$ and $C_{t,2}$ (centres of the nonwetting fluid-filled throats) to determine the angle between the throats (α). This angle is then used in conjunction with the advancing contact angle (Θ) and the pore radius (r) to trigonometrically determine the radius of curvature (R) of the meniscus, allowing for the determination of the invasion-Pc.

### *3. Snap-off*

In order to calculate the invasion-Pc of snap-offs, the geometry of the throat and the advancing contact angle are used along with the distance that the arc menisci must travel before they meet and cause the instability that results in the snap-off [16]. To determine this distance, the model uses the receding contact angle as well as the maximum meniscus curvature reached during the preceding drainage. The throats are assumed to be triangular in cross-section. The equations to calculate the invasion-Pc from this information can be found in the supplementary material [58].

## III. Materials and Methods

FIG. 3 contains a flowchart showing the workflow developed and used in this paper. The steps are elaborated on in this section.

Corresponding author: Sharon Ellman, sharon.ellman@ugent.be

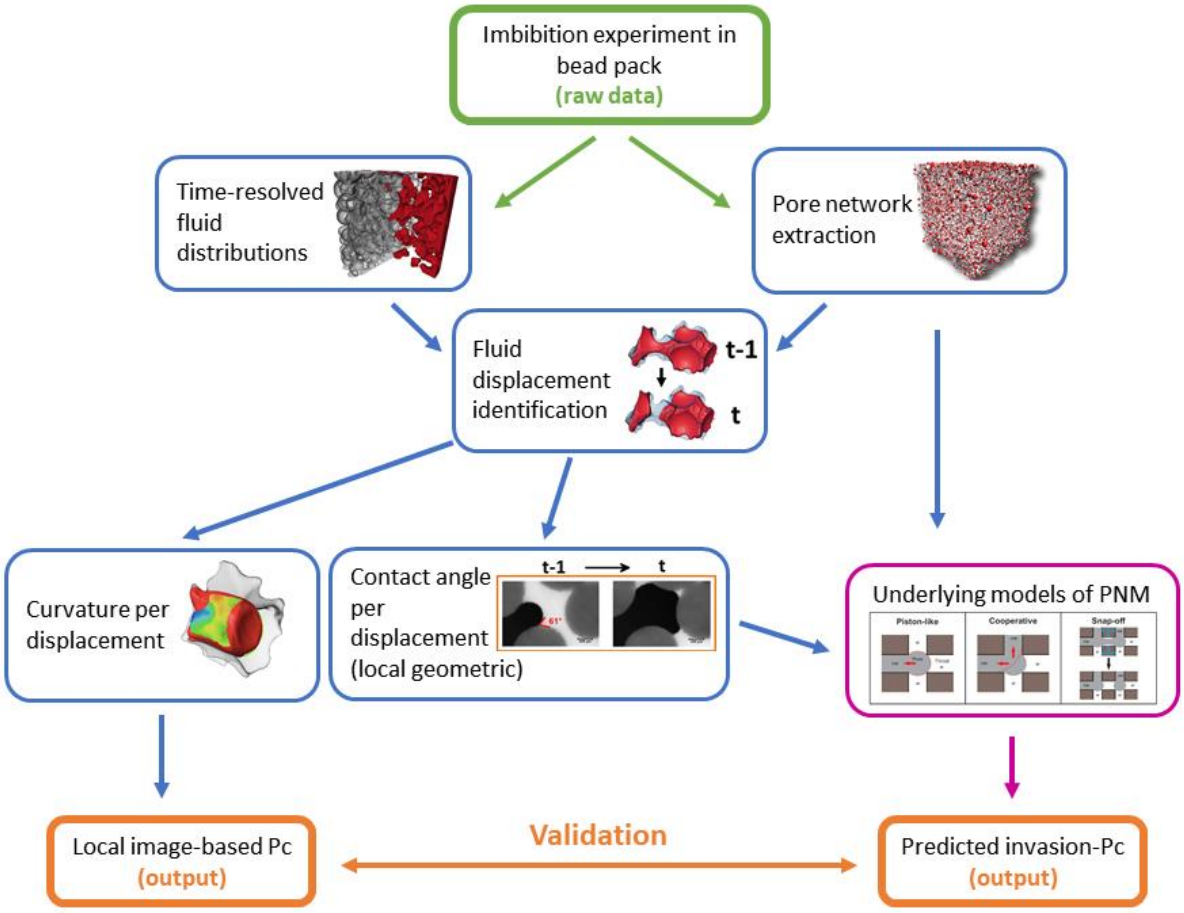


FIG. 3. Workflow of the methodology used.

## A. Experimental data

To verify imbibition PNMs, we compared model-predicted invasion-Pc values to fluid-fluid interfacial curvature measurements on µCT images of fluid distributions during imbibition. To do this, we assessed the local Pc-values calculated from these curvatures (resulting in 'local image-based Pc') and contact angle measurements in individual pores, determined from time-resolved µCT images. The experimental data came from an imbibition experiment in a glass beads pack, consisting of a mixture of beads of different diameters (0.6 to 1.4 mm). The experiment was carried out by Schlüter et al [39], at the GSECARS beamline of the Advanced Photon Source at the Argonne National Laboratory in the USA. The experiment consisted of an unsteady-state injection of wetting fluid into a cylindrical sample containing nonwetting fluid, directly after primary drainage. A summary of the experimental parameters can be found in TABLE I. The dataset had a temporal resolution high enough to identify most fluid displacements on a pore-by-pore basis and a spatial resolution high enough to resolve the curvature of the fluid menisci. It also contained external pressure transducer measurements, which were used to validate the curvature measurements. Capillary dominated flow was ensured by injecting at low flow rates. This time-resolved µCT experiment resulted in a series of 3D segmented images. Each image corresponds to the fluid distribution in the pore space at a discrete time during the experiment. The segmentation provided by Schlüter et al. [39], which was made with a modified form of Markov random field segmentation [39], was used. The relatively simple nature of the pore space of the bead pack facilitated the development of the workflow presented in this work. It should however be noted

Corresponding author: Sharon Ellman, sharon.ellman@ugent.be

that a glass bead pack is a simplified proxy for a real porous rock, and effects of this on the outcome of the validation study cannot be excluded.

TABLE I. Overview of the dataset used in the image analysis.

| Parameter | Value |
|---|---|
| Sample Dimension | 5.8 mm dia. x 7 mm long |
| Volume of sample used in analysis | 128 $mm^3$ (4.8 mm in length) |
| Boundary condition | Constant flow rate |
| Fluids | n-dodecane, CsCl-brine |
| Interfacial tension | 36 mN/m |
| Flow rate | 20 µl/h |
| Capillary number | $10^{-8}$ |
| Number of timesteps | 52 |
| Time per time step | 113 s |
| Time span (hr:min:sec) | 2:37:16 |
| Reconstructed voxel size | 8.4 µm |
| Pumped volume | 54.1 µl |
| Reference | Schluter et al.[39] |

## B. Image analysis

The 3D segmented imbibition images were analysed to obtain a characterisation of the pore space geometry as well as local curvature and contact angle measurements. The workflow used for the image analysis is inspired by the workflow for contact angle analysis during drainage described in Mascini et al. [31]. To test the invasion-Pc models discussed in Sec. II D, two different pore network models were extracted from the dry scan of the sample. The same networks were used to identify fluid displacements in individual pores in the experiment, forming the basis for local contact angle and curvature measurements. The contact angles were then used as inputs for the PNMs described above, and the curvatures were used to compare the invasion-Pc predictions for the given pore geometry and contact angle to the experiment. This workflow is described in detail below.

### *1. Pore network extraction*

The first step in the analysis was to divide the pore space into individual pores which are separated by narrower regions called throats. This extraction of the pore network causes a loss of geometric detail, but allows the complicated process of fluid invasion to be simplified and analysed more easily. This was done using (A) “pnextract” (an open source algorithm developed at Imperial College London [59], which employs a watershed algorithm using the maximum inscribed spheres to find the seeds); and (B)by using a watershed segmentation performed in Avizo 2020.3 (Thermo-Fisher Scientific) and feeding this into the open source python package “porespy” [60] to produce a pore network. The first extraction (pore network extraction A) consists of 604 pores and 2011 throats, while the second (pore network extraction B) consists of 393 pores and 1429 throats. Pore network extraction B consists of less pores than extraction A by design, as we wished to obtain an extraction in which fewer pores were over-separated. The largest inscribed spheres of the pores and the throats were found for both cases. The radii of the pores and throats were determined as the radii of the inscribed spheres in the pore and throat centre points. These pore network extractions served a dual purpose: firstly, they formed the basis of local fluid displacement detections, and secondly, they provided the pore space geometry characterisation needed as input for the PNMs.

### *2. Fluid displacement identification*

In order to assess the filling states of the pores and throats, their inscribed spheres were overlaid on the imbibition dataset (after it was registered to the dry scan of the sample). The fluid occupancy of the centre (bulk) of each pore or throat was then determined by whether the majority of the voxels in its inscribed sphere were filled with wetting fluid or nonwetting fluid. We did this for every pore and

Corresponding author: Sharon Ellman, sharon.ellman@ugent.be

throat in every timestep, using Avizo 2020.3. A fluid displacement was then identified when the occupancy of a pore changed from nonwetting to wetting fluid in a certain time step. Connected pores which changed occupancy in the same timestep were grouped into the same fluid displacement (FIG. 4). This was done in MATLAB using a graph-based connectivity clustering of the pores filled in each timestep. The pores and throats neighbouring the displacement were also recorded. The source pore for each displacement was assumed to be the pore within the invaded region with the largest radius. This works under the assumption that it is most difficult for the meniscus to move through the largest pore and hence this largest pore determines the threshold Pc needed for the displacement to proceed. In an invasion-percolation framework, this is the pore which determines the invasion-Pc, hence the radius of this pore is used in the PNM-based invasion-Pc models. Once the displacements were identified, they were then classified as piston-like displacements or cooperative pore-fillings, by assessing the occupancy of the throats surrounding the displacement in the timestep prior to its occurrence. Snap-offs in throats were identified as throats which changed occupancy while their two neighbouring pores remained filled with nonwetting fluid. The result of the fluid displacement identification was a list of categorised imbibition displacements with accompanying details on time and location at which they occurred, surrounding pores, etc.

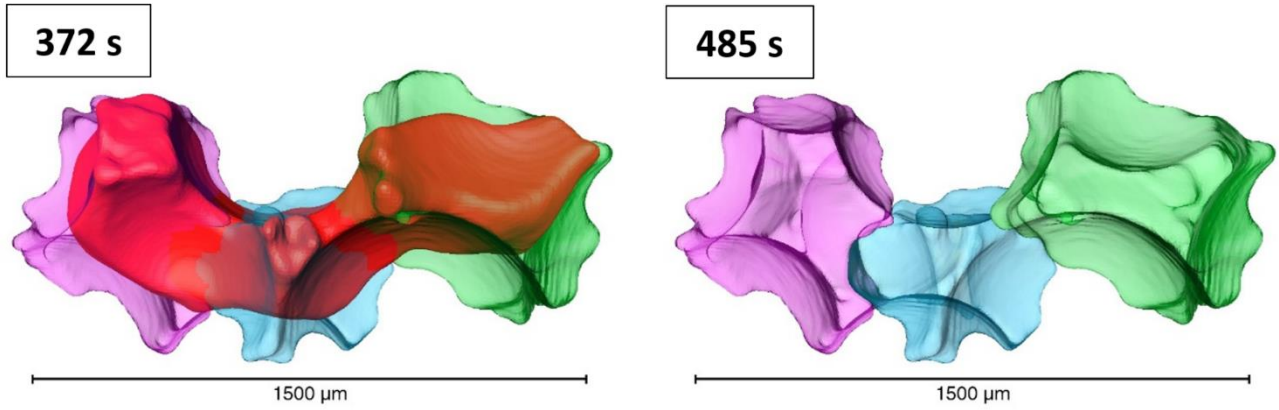


FIG. 4. An example of a multi-pore event. The three pores are transparent and are coloured in pink, blue and green (all grey in black and white), while the opaque red (dark grey in black and white) is the oil. At 372 s, the pores are filled with oil, while at 485 s the oil has been displaced by brine. Since the oil was displaced from all three pores in the same timestep, they were classified as a single displacement. These times represent consecutive scans taken during the experiment.

### *3. Curvature measurements*

To determine the curvature of the fluid menisci, the fluid/fluid interface was extracted as a triangulated surface from the three-phase segmented image at each timestep, using the marching cubes algorithm in Avizo 2020.3 [61]. Consequently, constrained smoothing using a Gaussian filter with a smoothing extent of three voxels was performed in Avizo 2020.3. This method is analogous to that of Li et al. [62]. The mean surface curvature was then determined from the Eigenvectors and Eigenvalues of a quadratic form which was locally fitted to the extracted surface. The image resolution limits the accuracy of this computation, especially in regions where the partial volume effect is especially pronounced, such as near the three-phase-contact-line [6]. To account for this, the data points were filtered based on two criteria. First, all curvatures corresponding to a radius of curvature smaller than 2 voxel sizes were omitted as these most likely represented noise. Then, data points were filtered based on their geodesic distance to the edge of the surface, i.e. points closer than 20% of the maximum geodesic distance were omitted. These distances were determined using the shortest edge distance algorithm [63]. Within each pore, the remaining datapoints were then weighted based on their geodesic distance (points further away from the grain surface were given a greater weighting) and the mean curvature per pore per timestep was calculated. To find the local curvature as closely as possible before

Corresponding author: Sharon Ellman, sharon.ellman@ugent.be

a filling event (i.e. a meniscus reconfiguration), we averaged the curvatures in the pores in the displacement as well as in the neighbouring pores in the time step immediately prior to its occurrence. This resulted in a single curvature estimate for each displacement.

#### *4. Contact angle determination*

Wettability, which is characterised by contact angle, has been found to vary in space, even within homogeneous materials such as that used in this study [64]. Our aim was to validate predictions of the invasion-Pc of individual fluid displacements, which depend in part on the effective contact angle of that specific displacement. This is why using a method which measures contact angles locally within the pore space was necessary. We compared conventional geometric contact angles to local geometric contact angles. These methods are briefly summarized below.

*(a) Geometric contact angles.* Geometric contact angles have been measured on µCT data by Andrew et al. [36], where the angle between the fluid-fluid interface and the solid surface was measured manually in the plane perpendicular to the three-phase-contact-line. This method was then enhanced by automated algorithms which find the geometric contact angle at every point on the three-phase-contact-line in the entire pore space [37,43,44,65]. The code developed by AlRatrout et al. [37] was used to calculate the conventional geometric contact angle distribution, which was determined from a single 3D image at the end of imbibition.

*(b) Local geometric contact angles.* These were introduced by Mascini et al. [31] and yield geometric contact angles locally in space and time. In this method, the code of AlRatrout et al. [37] is used in conjunction with a pore separation to determine a geometric contact angle in individual pores at the moment just before a fluid displacement takes place. This method was shown to reduce the uncertainty linked to the state of the interface caused by contact angle pinning. For a detailed description of the method, see Mascini et al. [31].

### C. Pc determination

#### *1. Curvature-based Pc measurement*

Image-based Pc values were determined from local menisci curvatures as there is a one-to-one relationship between the local Pc and the curvature of the fluid meniscus, which can be measured on the µCT images. Assuming the fluids are at quasi-equilibrium, the local curvature of the fluid-fluid interface at the time of displacement ($k_{thr}$) can be used to calculate the capillary pressure over the interface using the Young Laplace equation (2) and the interfacial tension (TABLE I). The local image-based Pc values determined by this method are used to validate the invasion-Pc values calculated from the PNMs.

$$Pc = 2\sigma k_{thr} \quad (2)$$

#### *2. Model implementation*

Displacements were identified and categorised during the image analysis, after which the different PNMs were used to estimate at which invasion-Pc values those displacements occurred. Because we determined the local fluid arrangement before each fluid invasion from the µCT images, we did not need to perform an entire PNM simulation to predict the invasion-Pc values that each displacement would occur at. For piston-like displacements, the local geometric contact angles and source pore radius were used to estimate the invasion-Pc. For cooperative pore-fillings, again the local geometric contact angles and source pore radius were used, as well as the filling states of the neighbouring throats, their relative position and their radii. Finally, in order to predict the invasion-Pc of snap-offs, the local geometric contact angles during imbibition and drainage were used, as well as the throat

Corresponding author: Sharon Ellman, sharon.ellman@ugent.be

radius; angles of the corners of the throat; and the maximum curvature obtained during the preceding drainage (see supplementary material [58]).

# IV. Results and Discussion

## A. Contact angles

By detecting changes in pore and throat occupancy during the experiment, we identified 146 distinct imbibition displacements. These displacements were used to calculate local geometric contact angles (FIG. 5). We also determined the conventional geometric contact angles as these have been used in several wettability studies [66–68]. Contact angles in such a system are dependent not only on the intermolecular forces between the fluids and the solid, but also on the geometry of the pore space [69]. This, in addition to measurement error, may account for the relatively high values of the contact angles measured in this dataset. The distribution of the local geometric contact angles was narrower than the conventional geometric contact angles, as is evident in FIG. 5 and the standard deviations in TABLE II. This suggests that the local geometric contact angles better account for the dynamics of the interface motion (such as hinging of pinned contact angles, hysteresis, interface relaxation, etc.) [31]. In this work, we investigate invasion-Pc linked to meniscus movements, hence it follows that the type of contact angle used must be equally local. For these reasons, the local geometric contact angles were selected for use as inputs in the PNMs in the following sections. To validate these measurements, manual geometric contact angles were determined in 6 randomly selected contact line points in the image (Figure S 2 in supplemental material [58]). Five were in good agreement with the results of the automated geometric contact angles in the same location, varying by 3˚ or less, with only one manual measurement differing from the automated value by 15˚. Due to the low flow rate of the experiment, some regions within the pore space may contain receding contact angles or contact angles at rest. The use of the local geometric contact angles addresses this issue and attempts to measure exactly the advancing contact angles, but the temporal resolution may mean that some measurements are made tens of seconds prior to the displacement occurring, adding to uncertainty.

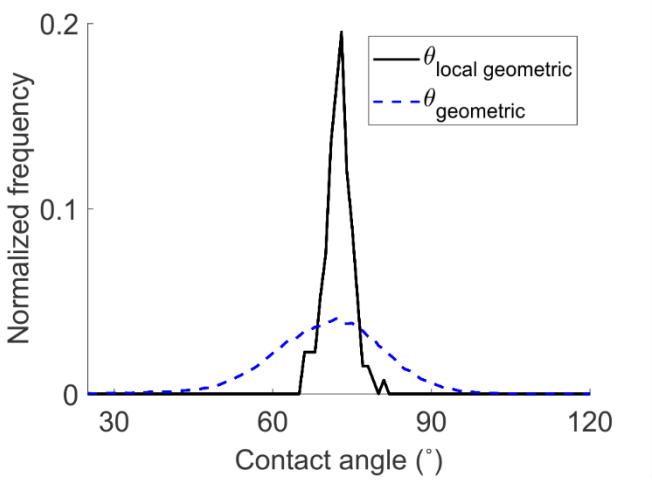


FIG. 5. A frequency distribution plot of contact angles measured during imbibition. The local geometric contact angles are measured locally in both space and time, while the geometric contact angles are measured on the final timestep of the experiment. The local geometric contact angles have the narrowest distribution, suggesting they have a higher precision and were therefore more suitable to use in the PNMs.

TABLE II. Means and standard deviations of contact angles.

| Contact angle type | Mean (°) | Standard deviation (°) |
|---|---|---|
| Local geometric | 72 | 2.6 |
| Conventional geometric | 70 | 10.9 |

Corresponding author: Sharon Ellman, sharon.ellman@ugent.be

## B. Validation of image-based curvatures

To assess the reliability of the meniscus curvatures from the µCT images, the local image-based Pc was compared to the average $P^c$ measured with a pressure transducer [6] (FIG. 6). The image-based results are in reasonable agreement with the pressure measurements. The image-based Pc-measurements are currently the only existing method to asses Pc locally in space and time at the pore scale, yet do come with several uncertainties. The presence of pendular rings of wetting fluid, as described in Armstrong et al. [6], may account for the mismatch between local image-based Pc and externally measured average $P^c$ seen at higher saturations. Curvature measurements on pendular rings commonly lead to severe underestimation of the capillary pressure, as their small size makes them sensitive to segmentation errors which can cause the improper reversal of curvature values from positive to negative [6]. Some scatter of the local image-based Pc around the pressure transducer readings was expected due to local variations in the pressure difference, as the fluids were not in equilibrium during the imbibition process [51]. The finite image resolution and the image analysis further added to uncertainty. Akai et al. [70] postulated that the local image-based Pc could be estimated to within 11% if the average radius of curvature is at least 10 times the image resolution. This radius of curvature equated to a local Pc of ~0.4 kPa in this study. Since pressure transducer readings were close to this value, the spatial resolution likely influenced the results, especially at lower wetting fluid saturations, where the radii of curvatures were smaller (due to the higher local Pc values) [31]. The limited temporal resolution added to the uncertainty because the curvatures were potentially determined tens of seconds before the fluid displacements occurred. The average rate of change of the pressure transducer readings was ~3Pa per timestep, which yields an uncertainty of ~4% on the average local image-based Pc solely due to temporal resolution. Furthermore, this limitation also caused motion artefacts in the images [39].

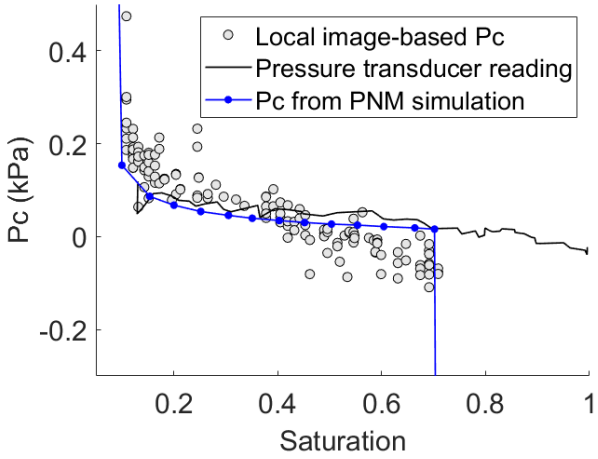


FIG. 6. Local image-based Pc based on curvature measurements and pressure transducer readings plotted against wetting fluid saturation as well as the Pc curve produced from a PNM simulation of imbibition in the glass bead pack.

## C. PNM simulation

There is some mismatch between the results of the PNM simulation of imbibition and the local image-based Pc (FIG. 6). The PNM simulation results were produced by conducting a simulation of imbibition in the maximum inscribed sphere pore network extraction, using the fluid distribution measured at the end of drainage in the experiment as the initial condition [7]. The models used in the simulation were derived from Valvatne and Blunt [16], using the implementation in the open source flow simulation code "pnflow" [59]. The simulation used the local geometric contact angles for each pore and utilised the mechanistic models described in Sec. II D. Invasion-Pc modelling. The Pc values produced by the simulation correspond to the lowest Pc needed to invade all the network elements that are

Corresponding author: Sharon Ellman, sharon.ellman@ugent.be

waterfilled at any given step during the simulation. The PNM predicted the displacement type to be: 26% snap-off, 72% piston-like displacement and 2% cooperative pore filling. The simulated Pc curve roughly matches the pressure transducer readings and local image-based Pc, with some mismatch. A potential contributor to this are dynamic effects. To investigate further reasons for mismatch, we used the mechanistic models to calculate the invasion-Pc for each distinct fluid distribution identified in the image analysis. Furthermore, to investigate the effect that contact angle plays on this PNM simulation, we simulated imbibition in this sample using several sets of contact angles (see supplemental material [58] Figure S 3 and Table 2). The resulting Pc curves show great sensitivity to contact angle, with the closest match to pressure transducer readings being achieved when using the local geometric contact angles.

## D. Fluid displacements

### *1. Piston-like fillings*

The results discussed from here onwards are for pore network extraction A, unless otherwise stated. The full set of results from pore network extraction B can be found in the supplemental material [58].

Of the 146 distinct displacements detected, 12 were classified as piston-like. For these displacements, the predicted invasion-Pc values followed the same trend as the local image-based values and the pressure transducer readings (FIG. 7): they decreased with increasing saturation, conforming to the conventional Pc imbibition curve [45]. However, the predicted invasion-Pc values were larger than the local image-based values (FIG. 8). This disparity was observed with both pore network extraction methods (FIG. 7), suggesting a systematic error.

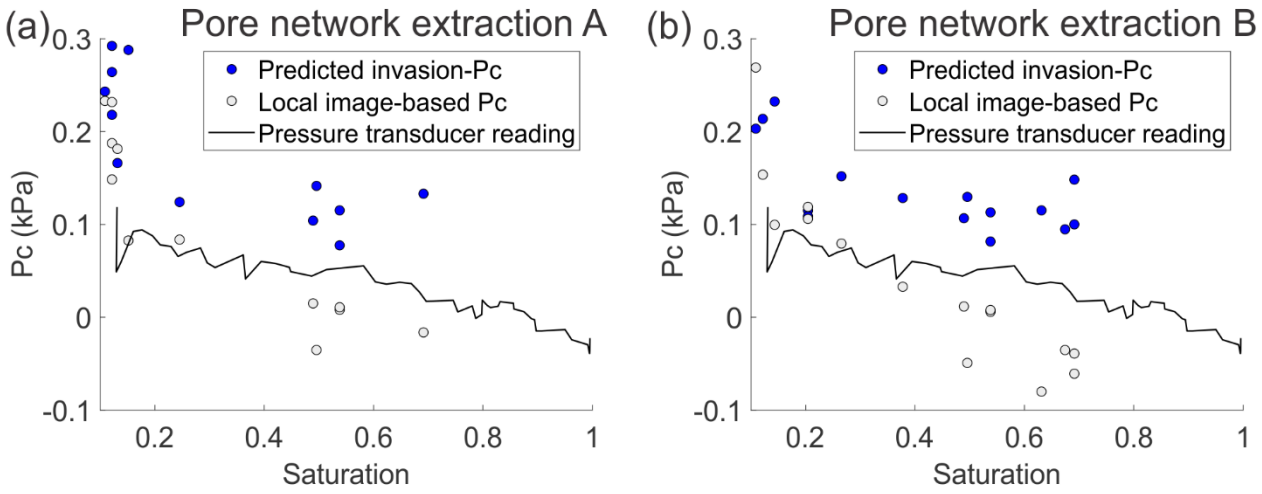


FIG. 7. Predicted invasion-Pc based on the two different PNM structures for piston-like displacements plotted against saturation, compared with the local image-based Pc based on curvature measurements and the pressure transducer readings. The figure in (a) was obtained using pnextract and in (b) using a watershed segmentation in Avizo 2020.3.

Corresponding author: Sharon Ellman, sharon.ellman@ugent.be

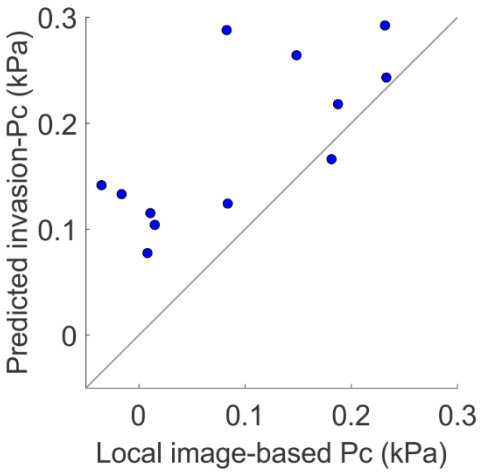


FIG. 8. Predicted invasion-Pc plotted against local image-based Pc using the maximum inscribed sphere pore network extraction.

Visual inspection of these displacements revealed that six occurred at the edge of the field of view (e.g., FIG. 9(a)) and thus no conclusions could be drawn from them. It further revealed that one displacement was in reality a cooperative pore filling that spanned two pores (FIG. 9(b)). The maximum inscribed sphere of the throat between the two pores was brine filled, yet in the region of the throat not encompassed by the sphere, oil was present. This hints at the difficulties of the PNM structure to allow the model to capture the intricacies of displacements spanning multiple pores. In this case, the interface configuration in the throat is what we traditionally expect to see in a pore, hence the model cannot recognise it as a cooperative pore filling, due to the way the pore space is divided into individual pores.

Visualizing the remaining five displacements revealed that the overestimation of the predicted invasion-Pc likely stemmed from difficulties the network structures have to accurately describe the pore space (FIG. 9(c) and (d)). Firstly, both network extractions over-separated the pore space: single pores were erroneously split into several pores (FIG. 9(c)). This yielded an underestimation of the radius used in the Young Laplace equation, resulting in higher than expected invasion-Pc values. At lower saturations, the invasion-Pc values were closer to the local image-based values and pressure transducer readings than at higher saturations. This was likely due to the fact that smaller pores were invaded first, and these pores were less likely to be over-separated than the larger pores filled later. Secondly, the radius used in the Young-Laplace equation was derived from the maximum inscribed sphere of the pore. This value was likely smaller than the maximum mean radius of curvature a meniscus could assume in irregularly shaped pores (FIG. 9(d)), again leading to higher than expected invasion-Pc values. The predicted invasion-Pc values of these displacements using pore network extraction B, were lower than for extraction A, likely because the former is less over-separated (see Table 1 in supplemental material [58]). These issues suggest that the network extraction methods struggled with describing the geometrical properties of the pore space of the sample in this case study.

Corresponding author: Sharon Ellman, sharon.ellman@ugent.be

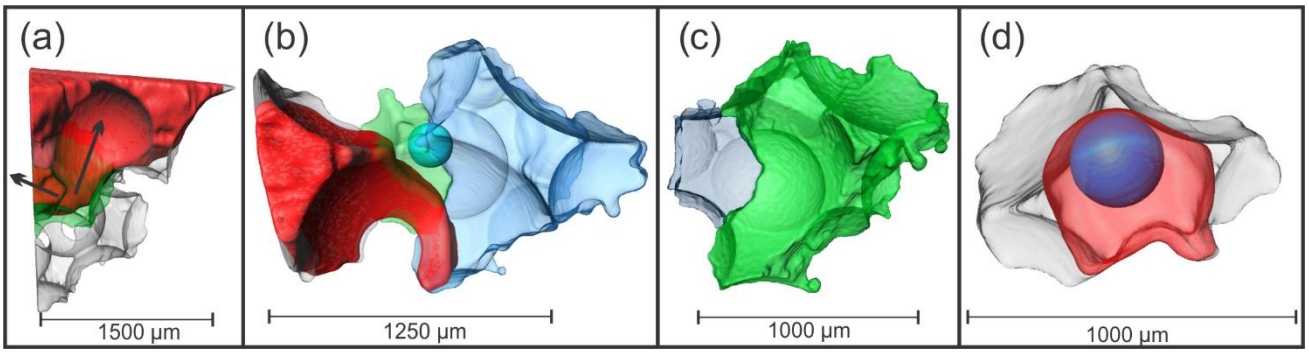


FIG. 9. This figure illustrates some sources of mismatch between predicted invasion-Pc and the local image-based Pc. (a) The oil in the green (middle) pore can escape in the direction of the left arrow or the right arrow. The right arrow's path is captured by the maximum inscribed sphere of the throat between the green pore and its neighbour, but there is no throat assigned at the location of the left arrow since it leads to outside the field of view. We can therefore make no conclusions from this displacement. (b) The throat between the green pore (left) and the blue pore (right) is represented by the blue ball at their boundaries. The filling state of that ball determines whether the throat is classified as containing oil or brine. Since the ball is devoid of oil, this throat was classified as brine filled, whereas there is oil in the lower part of the throat. (c) An over-separated pore. The pore network extraction results in what should be one pore being split into the green (right) and blue (left) pores. (d) The radius of curvature of the inscribed sphere (blue) is smaller than the radius of curvature of the oil protrusion (transparent red) within the pore (grey). The pore body is constrained by the pore walls in the axis running into and out of the page, which are not shown.

Another possible source of mismatch is the quasi-static nature of the PNM, meaning it does not intrinsically account for dynamic effects which occur during imbibition. While the experiment was unsteady-state [31], the capillary number of the flow was $10^{-8}$, suggesting that the fluids remained near hydraulic equilibrium [39]. Despite the low capillary number, viscous dynamic effects during rapid fluid reconfigurations could further explain the mismatch between the prediction and the measurement. Individual displacements during imbibition have been shown to occur at high velocities, possibly triggering fluid distributions and resulting in large local viscous forces, even when the average flow velocity is low and the capillary number hence indicates a capillary dominated flow [34]. Furthermore, the model was not explicitly created for bead packs. The distinct nature of bead packs, such as, their high level of smoothness compared to other porous materials; the small aspect ratio between their pores and throats; and the relatively little opportunity for thin film flow [39], may impact the results.

To investigate the effect of contact angle on these results, we conducted a sensitivity analysis (supplemental material [58] Figures S 12 – S 15). For piston-like fillings, using contact angles lower than the local geometric contact angle (mean 72°) leads to Pc values which are even more over-estimated (supplemental material [58] Figures S 12 and 13). Using 80° produces Pc values only marginally closer to the pressure transducer and local image-based values. In this work we elect to keep using the local geometric contact angles to avoid reducing contact angle to merely a tuning parameter.

The results indicate that the PNM would have predicted a different filling sequence than the one identified by the image analysis and curvature measurements. For some displacements, while their predicted invasion-Pc was higher relative to other displacements, their local image-based Pc was lower. This means the PNM would have predicted them to occur in a different sequence than the curvatures suggest. Also, some displacements have invasion-Pc values higher than displacements which were identified at lower saturations, meaning the PNM would have predicted them to occur earlier than was determined in the image analysis. Overall, this may affect the constitutive properties predicted by the PNM (e.g. relative permeability).

### *2. Cooperative pore-filling*

Of the 121 cooperative pore-fillings identified, 68 were one pore in size and could therefore be compared to model predictions (the investigated model is not valid for displacements where multiple

Corresponding author: Sharon Ellman, sharon.ellman@ugent.be

neighbouring pores are filled at the same time). Using both PNM structures, the predicted invasion-Pc values for these events were all negative and fell below the local image-based Pc values (FIG. 10(a)). Capillary pressure curves in quasi-static PNM are calculated as the minimum Pc needed to perform all the invasion up to a certain saturation, and the predictions are thus poor. Since invasion-percolation fills accessible network elements in the order of decreasing invasion-Pc, this means that the model would not expect the experimentally observed displacements to take place. The mismatch between the model and the experiment could be explained, at least in part, by taking into account the limited time resolution of the experiment: the invasions that appeared to be cooperative pore fillings could actually have taken place as a rapid succession of several displacements. This would entail one or more snap-offs occurring in the throats neighbouring the pore in question, quickly followed by a lower order cooperative pore-filling or piston-like displacement made accessible by the snap-off's alteration of the local fluid distribution. In an invasion-percolation framework, this sequential event could be more likely than the initially identified cooperative pore filling. This would be the case if the invasion-Pc of one or more snap-offs in the surrounding throats were higher than that of the latter.

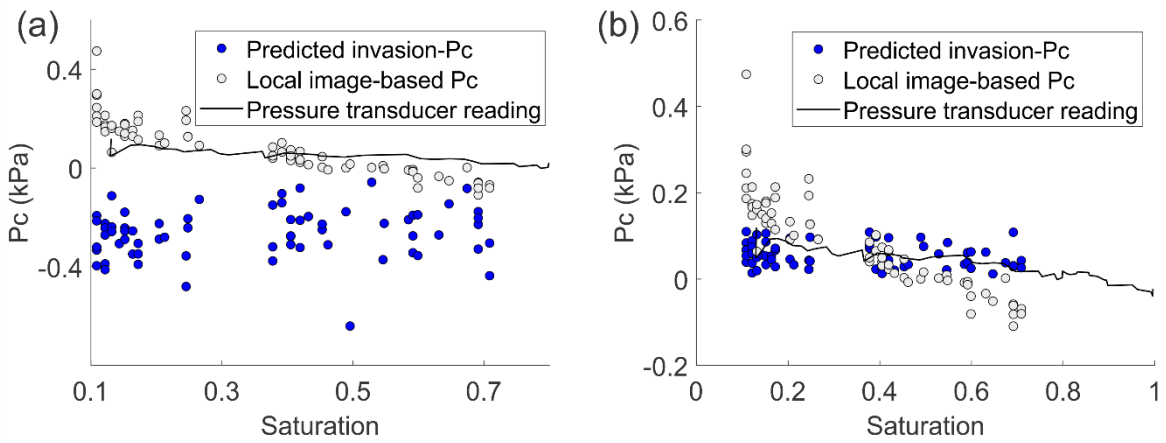


FIG. 10. (a) Predicted invasion-Pc for cooperative pore-fillings plotted against saturation, compared with the local image-based Pc and the pressure transducer readings. (b) Predicted invasion-Pc of snap-offs simulated around pores assumed to be filled by cooperative pore-fillings. According to percolation invasion, since they are greater than the predicted invasion-Pc values in (a), the model would predict them to occur. These values are for pore network extraction A. Pore network extraction B followed a similar trend; the corresponding figure can be found in the supplemental material Figures S 5 and S 6.

To test the impact of the possible occurrence of fast sequential events on the match between model and experiment, we calculated the invasion-Pc values of snap-offs surrounding the pores. Once the likelihoods of the snap-offs were confirmed, the invasion-Pc values of the pores were recalculated using the updated fluid configurations; e.g. if snap-off in a throat had a higher invasion-Pc than the cooperative pore filling, then that throat was reclassified as brine-filled, and the cooperative pore filling pressure for the neighbouring pore was recalculated. If snap-off in a throat had a lower invasion-Pc than the cooperative pore-filling, the throat remained classified as oil-filled. Depending on the updated fluid configurations, the predicted invasion Pc values were either calculated using the piston-like filling method or using the cooperative pore-filling method. We found that the predicted invasion-Pc values for the snap-offs were scattered around the local image-based values and the pressure transducer readings (FIG. 10(b)), suggesting that the model could have predicted them to occur. After simulating between one and seven snap-offs around each pore (TABLE III), the predicted invasion-Pc values matched better to the local image-based Pc values and pressure transducer readings (FIG. 11). Nevertheless, there was still scatter, which would cause the predicted invasion sequence to be different than the experimentally measured one. This could have an impact on the resulting constitutive properties that the PNM would predict. The predicted invasion-Pc values were again

Corresponding author: Sharon Ellman, sharon.ellman@ugent.be

greater than the local image-based Pc values (FIG. 11). The reasons for mismatch between the model and the experiment are likely the same as for the mismatch in the piston-like displacements: the pore separation methods were unable to accurately describe the pore space and the quasi-static nature of the model potentially failed to capture dynamic effects sufficiently.

TABLE III. Number of snap-offs simulated and the corresponding number of pores where predicted invasion-Pc has just become greater than (or near to) local image-based Pc.

| Number of snap-offs | Number of pores where predicted invasion-Pc has just become greater than local image-based Pc |
|---|---|
| 1 | 27 |
| 2 | 20 |
| 3 | 13 |
| 4-7 | 8 |

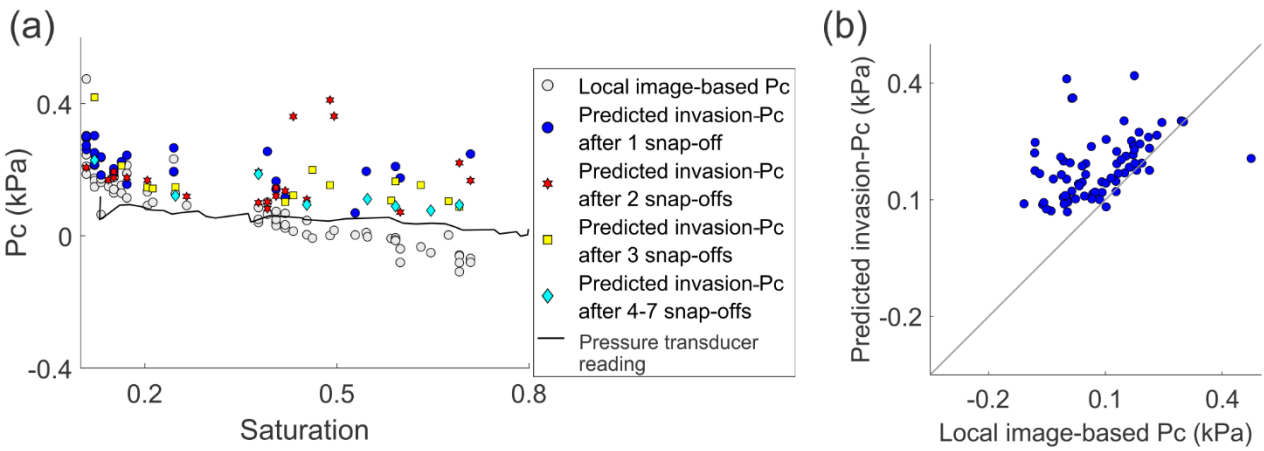


FIG. 11. These graphs show the results after snap-offs were simulated. (a) Predicted invasion-Pc for cooperative pore-fillings plotted against saturation, compared with the local image-based Pc and the pressure transducer readings. (b) Predicted invasion-Pc for cooperative pore-fillings plotted against local image-based Pc. These values are for pore network extraction A. Pore network extraction B followed a similar trend; the corresponding figure can be found in the supplemental material Figures S 7 and S 8.

If we assume the sequential filling approach outlined above to be realistic, we find that there were 147 snap-offs, 64 piston-like displacements and 4 cooperative pore-fillings (FIG. 12). This means that 64 displacements occurred with one neighbouring throat filled with oil and four displacements occurred with two neighbouring throats filled with oil (i.e. as $I_2$ displacements). The dominance of snap-offs and piston-like fillings over cooperative pore fillings agrees with the PNM simulation (see Section IV.C PNM simulation), however the simulation predicted more piston-like fillings than snap-offs unlike these findings. This dominance of piston-like displacements compared to cooperative pore-fillings agrees partly with the findings of Singh et al. [71] who reported 68% piston-like displacements and only 22% $I_2$ cooperative pore-fillings when analysing capillary dominated imbibition in a Ketton limestone rock sample. Our findings showed a much higher proportion of piston-like displacements compared to cooperative pore-fillings than Singh et al. [71], however. Singh et al. [71] also found a lower percentage of snap-offs (~7% of displacements), despite the typically higher aspect ratios in Ketton limestone compared to a glass bead pack. This could be due to misidentification of fast sequential events in the former, as they suffered from similar time resolution constraints as the experimental data presented here. We would expect the high number of snap-offs to lead to extensive trapping, which is not seen in the experimental results. A possible reason for this is that the bead pack is highly connected, so oil adjacent to a snap-off may remain part of the connected oil phase via a throat which is still oil-filled.

Corresponding author: Sharon Ellman, sharon.ellman@ugent.be

Further experiments with higher temporal resolution are needed to validate our assumption, especially since it is unexpected for so many snap-offs to occur in a bead pack. Again, since the models were not created explicitly with bead packs in mind, their distinct nature may have had an effect on the results.

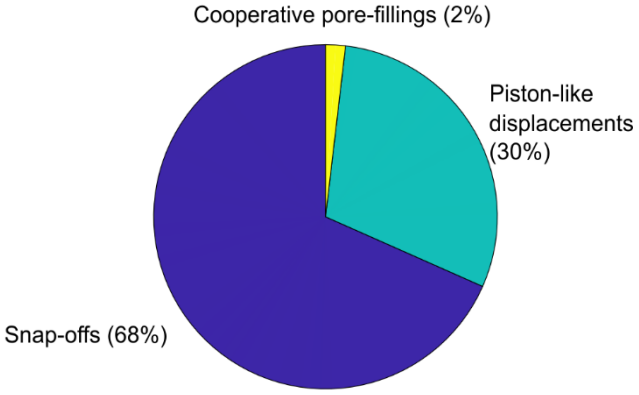


FIG. 12. Proportions of the different types of displacements assuming the sequential filling approach is realistic. The original 68 single pore cooperative pore-fillings were thus found to be this combination of different displacement types. These values are for pore network extraction A. Pore network extraction B followed a similar trend; the corresponding figure can be found in the supplemental material Figures S 9.

The cooperative pore fillings were sensitive to the contact angle supplied to the model (supplemental material [58] Figure S 14). When using lower contact angles (i.e. 0° to 50°), more of these displacements were predicted to have positive invasion-Pc values without assuming surrounding snap-offs. However, these values strongly over-estimated predicted invasion-Pc. As contact angles were increased, more and more of these displacements were predicted to only occur at negative invasion-Pc values.

We reach very similar conclusions for pore network extraction B (Figures S 7 and S 9 in the supplemental material [58]). While the predicted invasion-Pc values are slightly lower using extraction B, they are still well above the local image-based Pc and pressure transducer readings. Furthermore, the proportions of different types of displacements is almost identical for the two pore network extractions. While extraction B seems to be performing marginally better than extraction A, the same systematic errors are present.

The pores filled in the simulation (FIG. 6) are not necessarily the same as during the experiment, explaining why the mechanistic models for piston-like fillings and cooperative pore-fillings overestimate predicted invasion-Pc (FIG. 7 and FIG. 11), while the results from the simulation do not show this trend. This is because the simulation calculates the invasion-Pc for all accessible pores and then fills the one with the highest invasion-Pc. If this sequence of filling is different than that in the experiment, then constitutive properties such as relative permeability may potentially not be captured.

### *3. Snap-off*

Of the 13 snap-offs identified by the image analysis, one was eliminated as an outlier as it had a predicted invasion-Pc several orders of magnitude larger than that of the other snap-offs. The invasion-Pc values loosely followed the expected trend of decreasing Pc with increasing saturation (FIG. 13). However, this trend was not visible in the local image-based Pc values, likely due to scatter. The local image-based Pc values of snap-offs are most difficult to estimate as there are no terminal menisci on which to make curvature measurements before the displacement. Instead measurements were made

Corresponding author: Sharon Ellman, sharon.ellman@ugent.be

in the timestep after the displacement, increasing the uncertainty of the measurement. We found that the predicted invasion-Pc values were scattered around the local image-based values, suggesting that the model could have predicted them to occur. The low temporal resolution may contribute to the mismatch between the pressure transducer readings and the predicted invasion-Pc values, which were mostly lower than the former. The mismatch may also be due to the flow not being at capillary equilibrium. In order to study this, the temporal and spatial locations of the snap-offs were investigated.

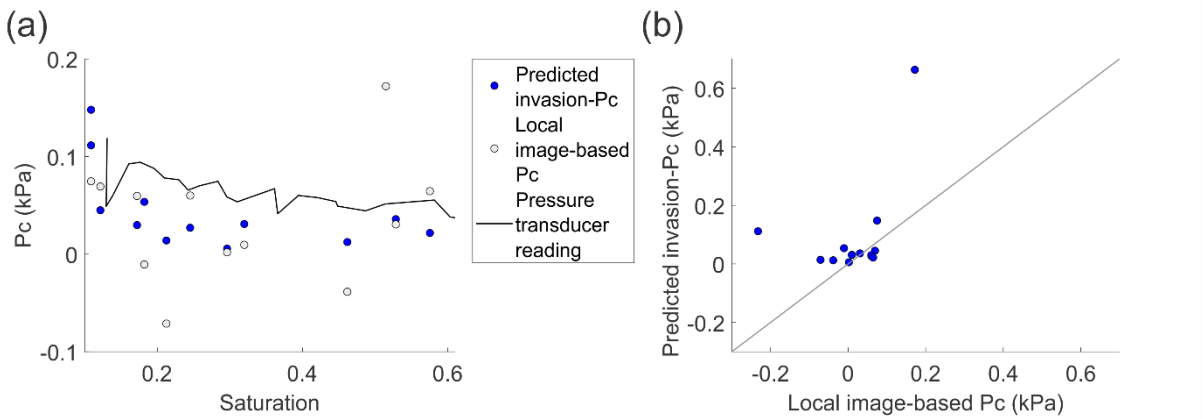


FIG. 13. (a) Predicted invasion-Pc for snap-offs plotted against saturation, compared with the local image-based Pc and the pressure transducer readings. (b) Predicted invasion-Pc for snap-offs plotted against local image-based Pc. These values are for pore network extraction A. Pore network extraction B followed a similar trend; the corresponding figures can be found in the supplemental material Figures S 10.

Snap-offs which occurred closer to the inlet happened earlier in the experiment and at lower saturations (FIG. 14). However, there is no increasing trend in the predicted invasion-Pc with the length along the sample. These results make sense when considering that brine must flow through films from the inlet to the location of the snap-off. This means that snap-offs at locations further from the inlet would happen later, and thus at higher saturation and lower invasion-Pc. These trends thus reflect that the sample was not at capillary equilibrium, and can thus not be captured by quasi-static models [45,51]. In our sensitivity study on contact angles supplied to the model (supplemental material [58] Figure S 15), we see greater over-estimation of snap-off predicted invasion-Pc for lower contact angles, again highlighting the sensitivity of the analysis to contact angle.

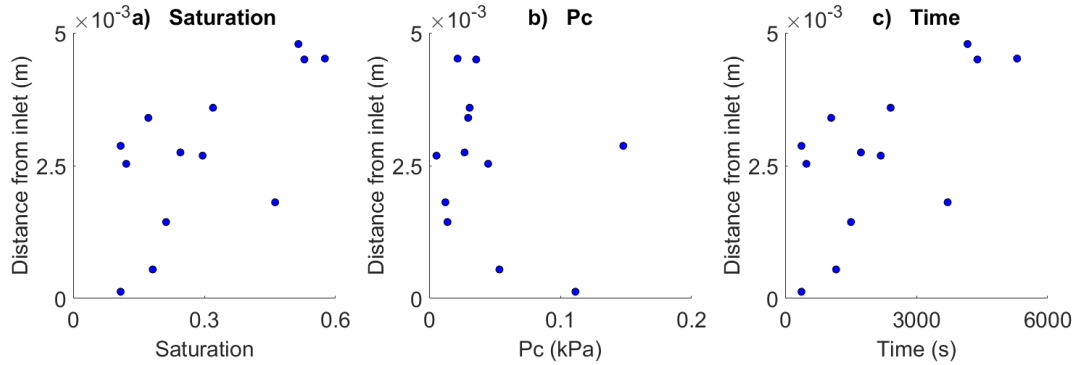


FIG. 14. Saturation, predicted invasion-Pc and time plotted against distance from the inlet for each snap-off identified in the image analysis. These values are for pore network extraction A. Pore network extraction B followed a similar trend; the corresponding figure can be found in the supplemental material Figures S 11.

Corresponding author: Sharon Ellman, sharon.ellman@ugent.be

# V. Conclusion

In this work, we developed a workflow to validate models of imbibition using invasion-Pc, which dictates the sequence in which the pore-filling process occurs. We did this by comparing invasion-Pc values predicted by PNMs of piston-like displacements, cooperative pore-fillings and snap-offs to local image-based Pc values calculated from meniscus curvatures extracted from µCT images. We considered two different PNM extraction methods from a dry µCT scan of the sample and measured the local geometric contact angles which were used as input to the models. Using this workflow on a µCT dataset of imbibition in a glass bead pack allowed us to investigate causes of error in these PNMs.

In the investigated PNMs, the invasion-Pc values predicted by the PNMs of piston-like displacements were all greater than the local image-based Pc values. Possible reasons for this include: uncertainties in the experimental analysis of the data, difficulties of the used network extraction methods to accurately describe the pore space geometry (particularly due to over-separation of pores) and viscous/dynamic effects. Due to the relatively low temporal resolution, we worked under the assumption that sequential events were realistic and saw the same trends in the invasion-Pc values predicted for cooperative pore-fillings as in the piston-like displacements. However, the PNM predicted that piston-like displacements were more plentiful than $I_2$ cooperative pore-fillings, aligning in part with the findings of Singh et al. [71]. This shows that while the investigated PNM were capable of capturing the general prevalence of the different types of displacements, they failed to match predicted invasion-Pc values to local image-based Pc values for specific displacements. The results were sensitive to errors in the geometrical description of the pore space, hence highlighting the importance of accurately describing this during network extraction. In the presented bead pack dataset, this might have been more problematic than in pore geometries with higher constriction ratios, where throat surfaces may be more easily identified and where cooperative pore filling might play a less important role [72]. Finally, as the investigated PNM was quasi-static in nature, viscous/dynamic effects likely also played a role. The predicted invasion-Pc values for snap-offs were again all greater than the local image-based Pc values. This may be attributed to the relatively low temporal resolution of the dataset and dynamic effects. The correlations observed between the distance from the inlet and the saturation, predicted invasion-Pc and time at which snap-offs occurred further suggests that the sample was not at capillary equilibrium. We reached very similar conclusions for pore network B, which seemed to be performing marginally better than extraction A due to having less over-separation of pores, yet still showed the same systematic errors. Previous work shows similar or better agreement between predicted invasion-Pc and macroscale measurements than we see in this work, likely because here, we treat contact angle as a parameter to be measured directly from the experimental images on a pore-by-pore basis, unlike most previous studies where contact angles are tuned to match the Pc curve. Future work will include using this workflow on geological porous material, as the results here could have been affected by properties distinct to bead packs.

In order to accurately predict relative permeabilities and other constitutive properties, PNMs rely on the predicted invasion-Pc values in individual pores and throats leading to the correct sequence in which displacements occur. Mismatches in these predictions could render the constitutive properties predicted by PNMs inaccurate. In our results, the predicted and measured Pc curves matched relatively well despite observing mismatches in individual invasion-Pc calculations. However, the PNM overestimated the amount of trapping, and the difference in filling sequences may be reflected in other properties such as the relative permeability, warranting further validation studies investigating such properties. The method presented here may be used to guide the development of improved pore network extraction methods that optimally capture the link between local pore geometry and fluid invasions.

Corresponding author: Sharon Ellman, sharon.ellman@ugent.be

## Acknowledgements

Dr. Steffen Schlüter is thanked for making his data available. Sharon Ellman is a PhD Fellow with the Research Foundation – Flanders (FWO) and acknowledges its support under grant 1182822N. T. Bultreys holds a senior postdoctoral fellowship from the Research Foundation-Flanders (FWO) under Grant No. 12X0922N. This research also received funding from the Research Foundation–Flanders under grant G051418N. The reviewers are thanked for their useful comments which helped to improve the work.


## Data and workflow availability

The experimental data used in this work is freely available online (http://www.ufz.de/record/dmp/archive/4780). The code used to determine the geometric contact angles along the three-phase-contact-line is freely available online (https://github.com/AhmedAlratrout/ContactAngle-Curvature-Roughness). Pore network extraction A was performed using the open source algorithm "pnextract" (available at: https://github.com/ImperialCollegeLondon/pnextract). Pore network extraction B was performed using the separation module in Avizo 2020.3 (Thermo Fisher Scientific) with a "marker extent" of 2. This pore space separation was fed into the open source package PoreSpy to generate a pore network (https://porespy.org/). The pore network simulation was conducted using the open access code "pnflow" (available at: https://github.com/ImperialCollegeLondon/pnflow). The displacement identification code was written in MATLAB and is available on github (https://github.com/sharonellman1/Fluid-Displacement-Identification).

## VI. References


1. Fetter, C. *Contaminant Hydrogeology*. (Prentice Hall, 1999).
2. Kota, A. K., Kwon, G., Choi, W., Mabry, J. M. & Tuteja, A. Hygro-responsive membranes for effective oilg-water separation. *Nat Commun* **3**, (2012).
3. Ma, J., Li, Q., Kühn, M. & Nakaten, N. Power-to-gas based subsurface energy storage: A review. *Renewable and Sustainable Energy Reviews* **97**, 478–496 (2018).
4. Lackner, K. S. A Guide to CO2 Sequestration. *Science (1979)* **300**, 1677–1678 (2003).
5. Benson, S. M. & Cole, D. R. CO2 sequestration in deep sedimentary formations. *Elements* **4**, 325–331 (2008).
6. Armstrong, R. T., Porter, M. L. & Wildenschild, D. Linking pore-scale interfacial curvature to column-scale capillary pressure. *Adv Water Resour* **46**, 55–62 (2012).
7. Bultreys, T. *et al.* Verifying Pore Network Models of Imbibition in Rocks Using Time-Resolved Synchrotron Imaging. *Water Resour Res* **56**, 1–23 (2020).
8. Singh, K., Jung, M., Brinkmann, M. & Seemann, R. Capillary-dominated fluid displacement in porous media. *Annu Rev Fluid Mech* **51**, 429–449 (2019).
9. Zhao, B., MacMinn, C. W. & Juanes, R. Wettability control on multiphase flow in patterned microfluidics. *Proceedings of the National Academy of Sciences* **113**, 10251–10256 (2016).


Corresponding author: Sharon Ellman, sharon.ellman@ugent.be

10. Bultreys, T., De Boever, W. & Cnudde, V. Imaging and image-based fluid transport modeling at the pore scale in geological materials: A practical introduction to the current state-of-the-art. *Earth Sci Rev* **155**, 93–128 (2016).

11. Berg, S. *et al.* Connected pathway relative permeability from pore-scale imaging of imbibition. *Adv Water Resour* **90**, 24–35 (2016).

12. Liu, H. *et al.* Multiphase lattice Boltzmann simulations for porous media applications: A review. *Comput Geosci* **20**, 777–805 (2016).

13. Gostick, J. T., Misaghian, N., Yang, J. & Boek, E. S. Simulating volume-controlled invasion of a non-wetting fluid in volumetric images using basic image processing tools. *Comput Geosci* **158**, (2022).

14. Helland, J. O., Friis, H. A., Jettestuen, E. & Skjæveland, S. M. Footprints of spontaneous fluid redistribution on capillary pressure in porous rock. *Geophys Res Lett* **44**, 4933–4943 (2017).

15. Jettestuen, E., Friis, H. A. & Helland, J. O. A locally conservative multiphase level set method for capillary-controlled displacements in porous media. *J Comput Phys* **428**, (2021).

16. Valvatne, P. H. & Blunt, M. J. Predictive pore-scale modeling of two-phase flow in mixed wet media. *Water Resour Res* **40**, 1–21 (2004).

17. Lindquist, W. B., Lee, S. M., Coker, D. A., Jones, K. W. & Spanne, P. Medial axis analysis of void structure in three-dimensional tomographic images of porous media. *J Geophys Res Solid Earth* **101**, 8297–8310 (1996).

18. Bakke, S. & Øren, P. E. 3-D pore-scale modelling of sandstones and flow simulations in the pore networks. *SPE Journal* **2**, 136–149 (1997).

19. Youssef, S., Rosenberg, E., Gland, N., Bekri, S. & Vizika, O. Quantitative 3D characterisation of the pore space of real rocks: improved µ-CT resolution and pore extraction methodology. *Int. Symp. Soc. Core Analysts. Society of Core Analysts.* (2007).

20. Thompson, K. E. *et al.* Application of a New Grain-Based Reconstruction Algorithm to Microtomography Images for Quantitative Characterization and Flow Modeling. in *All Days* (SPE, 2005). doi:10.2118/95887-MS.

21. Silin, D. & Patzek, T. Pore space morphology analysis using maximal inscribed spheres. *Physica A: Statistical Mechanics and its Applications* **371**, 336–360 (2006).

22. Dong, H. & Blunt, M. J. Pore-network extraction from micro-computerized-tomography images. *Phys Rev E Stat Nonlin Soft Matter Phys* **80**, (2009).

23. Rabbani, A., Jamshidi, S. & Salehi, S. An automated simple algorithm for realistic pore network extraction from micro-tomography images. *J Pet Sci Eng* **123**, 164–171 (2014).

24. Wildenschild, D. & Sheppard, A. P. X-ray imaging and analysis techniques for quantifying pore-scale structure and processes in subsurface porous medium systems. *Adv Water Resour* **51**, 217–246 (2013).

25. Bondino, I., Hamon, G., Kallel, W. & Kac, D. Relative Permeabilities From Simulation in 3D Rock Models and Equivalent Pore Networks: Critical Review and Way Forward. *Petrophysics - The SPWLA Journal of Formation Evaluation and Reservoir Description* **54**, 538–546 (2013).

Corresponding author: Sharon Ellman, sharon.ellman@ugent.be

26. Blunt, M. J. *et al.* Pore-scale imaging and modelling. *Adv Water Resour* **51**, 197–216 (2013).

27. Bultreys, T. *et al.* Validation of model predictions of pore-scale fluid distributions during two-phase flow. *Phys Rev E* **97**, (2018).

28. Porter, M. L., Schaap, M. G. & Wildenschild, D. Lattice-Boltzmann simulations of the capillary pressure-saturation-interfacial area relationship for porous media. *Adv Water Resour* **32**, 1632–1640 (2009).

29. Joekar-Niasar, V., Prodanović, M., Wildenschild, D. & Hassanizadeh, S. M. Network model investigation of interfacial area, capillary pressure and saturation relationships in granular porous media. *Water Resour Res* **46**, (2010).

30. Øren, P. E., Bakke, S. & Arntzen, O. J. Extending Predictive Capabilities to Network Models. *SPE Journal* **3**, 324–335 (1998).

31. Mascini, A., Cnudde, V. & Bultreys, T. Event-based contact angle measurements inside porous media using time-resolved micro-computed tomography. *J Colloid Interface Sci* **572**, 354–363 (2020).

32. Berg, S. *et al.* Real-time 3D imaging of Haines jumps in porous media flow. *Proc Natl Acad Sci U S A* **110**, 3755–3759 (2013).

33. Armstrong, R. *et al.* Subsecond pore-scale displacement processes and relaxation dynamics in multiphase flow. *Water Resour Res* **50**, 9162–9176 (2014).

34. Rücker, M. *et al.* From connected pathway flow to ganglion dynamics. *Geophys Res Lett* **42**, 3888–3894 (2015).

35. Youssef, S. *et al.* 4D Imaging of Fluid Flow Dynamics in Natural Porous Media With Ultra-Fast X-Ray Microtomography. *International Symposium of Core Analyst,* 1–12 (2013).

36. Andrew, M., Bijeljic, B. & Blunt, M. J. Pore-scale contact angle measurements at reservoir conditions using X-ray microtomography. *Adv Water Resour* **68**, 24–31 (2014).

37. AlRatrout, A., Raeini, A. Q., Bijeljic, B. & Blunt, M. J. Automatic measurement of contact angle in pore-space images. *Adv Water Resour* **109**, 158–169 (2017).

38. Akai, T., Lin, Q., Bijeljic, B. & Blunt, M. J. Using energy balance to determine pore-scale wettability. *J Colloid Interface Sci* **576**, 486–495 (2020).

39. Schlüter, S. *et al.* Pore-scale displacement mechanisms as a source of hysteresis for two-phase flow in porous media. *Water Resour Res* **52**, 2194–2205 (2016).

40. Gharbi, O. & Blunt, M. J. The impact of wettability and connectivity on relative permeability in carbonates: A pore network modeling analysis. *Water Resour Res* **48**, 1–14 (2012).

41. Raeesi, B. & Piri, M. The effects of wettability and trapping on relationships between interfacial area, capillary pressure and saturation in porous media: A pore-scale network modeling approach. *J Hydrol (Amst)* **376**, 337–352 (2009).

42. Høiland, L. K., Spildo, K. & Skauge, A. Fluid flow properties for different classes of intermediate wettability as studied by network modelling. *Transp Porous Media* **70**, 127–146 (2007).

43. Klise, K. A., Moriarty, D., Yoon, H. & Karpyn, Z. Automated contact angle estimation for three-dimensional X-ray microtomography data. *Adv Water Resour* **95**, 152–160 (2016).


Corresponding author: Sharon Ellman, sharon.ellman@ugent.be

44. Scanziani, A., Singh, K., Blunt, M. J. & Guadagnini, A. Automatic method for estimation of in situ effective contact angle from X-ray micro tomography images of two-phase flow in porous media. *J Colloid Interface Sci* **496**, 51–59 (2017).

45. Blunt, M. J. *Multiphase Flow in Permeable Media: A Pore-Scale Perspective*. *Multiphase Flow in Permeable Media* (2017). doi:10.1017/9781316145098.

46. Lenormand, R., Zarcone, C. & Sarr, A. *Mechanisms of the displacement of one fluid by another in a network of capillary ducts*. *Transport in Porous Media* vol. 83 337 (1983).

47. Singh, K., Bultreys, T., Raeini, A., Shams, M. & Blunt, M. Imbibition in porous media: correlations of displacement events with pore-throat geometry and the identification of a new type of pore snap-off. 1–12 (2019) doi:10.31223/osf.io/62gfr.

48. Berg, S. *et al.* Real-time 3D imaging of Haines jumps in porous media flow. *Proc Natl Acad Sci U S A* **110**, 3755–3759 (2013).

49. Berg, S. *et al.* Connected pathway relative permeability from pore-scale imaging of imbibition. *Adv Water Resour* **90**, 24–35 (2016).

50. Haines, W. B. The hysteresis effect in capillary properties and the mode of moisture distribution associated therewith. *J. Agric. Science* **20**, 7 (1929).

51. Singh, K. *et al.* Dynamics of snap-off and pore-filling events during two-phase fluid flow in permeable media. *Sci Rep* **7**, 1–13 (2017).

52. Ferrari, A. & Lunati, I. Direct numerical simulations of interface dynamics to link capillary pressure and total surface energy. *Adv Water Resour* **57**, 19–31 (2013).

53. Wilkinson, D. & Willemsen, J. F. Invasion percolation: a new form of percolation theory. *J Phys A Math Gen* **16**, 3365 (1983).

54. Gladkikh, M. & Bryant, S. Prediction of interfacial areas during imbibition in simple porous media. *Adv Water Resour* **26**, 609–622 (2003).

55. Mason, G. & Morrow, N. R. Effect of Contact Angle on Capillary Displacement Curvatures in Pore Throats Formed by Spheres. *J Colloid Interface Sci* **168**, 130–141 (1994).

56. Friis, H. A., Pedersen, J., Jettestuen, E., Helland, J. O. & Prodanović, M. Pore-Scale Level Set Simulations of Capillary-Controlled Displacement with Adaptive Mesh Refinement. *Transp Porous Media* **128**, 123–151 (2019).

57. Ruspini, L. C., Farokhpoor, R. & Øren, P. E. Pore-scale modeling of capillary trapping in water-wet porous media: A new cooperative pore-body filling model. *Adv Water Resour* **108**, 1–14 (2017).

58. See Supplemental Material at [URL will be inserted by publisher].

59. Raeini, A. Q., Bijeljic, B. & Blunt, M. J. Generalized network modeling of capillary-dominated two-phase flow. *Phys Rev E* **97**, (2018).

60. Gostick, J. *et al.* PoreSpy: A Python Toolkit for Quantitative Analysis of Porous Media Images. *J Open Source Softw* **4**, 1296 (2019).


Corresponding author: Sharon Ellman, sharon.ellman@ugent.be

61. Lorensen, W. E. & Cline, H. E. Marching cubes: A high resolution 3D surface construction algorithm. *Proceedings of the 14th Annual Conference on Computer Graphics and Interactive Techniques, SIGGRAPH 1987* **21**, 163–169 (1987).

62. Li, T., Schlüter, S., Dragila, M. I. & Wildenschild, D. An improved method for estimating capillary pressure from 3D microtomography images and its application to the study of disconnected nonwetting phase. *Adv Water Resour* **114**, 249–260 (2018).

63. Dijkstra, E. W. A note on two problems in connexion with graphs. *Numer Math (Heidelb)* **1**, 269–271 (1959).

64. Quéré, D. Wetting and roughness. *Annu Rev Mater Res* **38**, 71–99 (2008).

65. Khanamiri, H., Slotte, P. A. & Berg, C. F. Contact Angles in Two - Phase Flow Images. *Transp Porous Media* **135**, 535–553 (2020).

66. Alhammadi, A. M., Alratrout, A., Singh, K., Bijeljic, B. & Blunt, M. J. In situ characterization of mixed-wettability in a reservoir rock at subsurface conditions. *Sci Rep* **7**, 1–9 (2017).

67. AlRatrout, A., Blunt, M. J. & Bijeljic, B. Spatial Correlation of Contact Angle and Curvature in Pore-Space Images. *Water Resour Res* **54**, 6133–6152 (2018).

68. AlRatrout, A., Blunt, M. J. & Bijeljic, B. Wettability in complex porous materials, the mixed-wet state, and its relationship to surface roughness. *Proc Natl Acad Sci U S A* **115**, 8901–8906 (2018).

69. Behnoudfar, D., Dragila, M. I., Meisenheimer, D. & Wildenschild, D. Contact angle hysteresis : A new paradigm? *Adv Water Resour* **161**, 104138 (2022).

70. Akai, T., Lin, Q., Alhosani, A., Bijeljic, B. & Blunt, M. Quantification of Uncertainty and Best Practice in Computing Interfacial Curvature from Complex Pore Space Images. *Materials* **12**, 2138 (2019).

71. Singh, K., Bultreys, T., Raeini, A. Q., Shams, M. & Blunt, M. J. New type of pore-snap-off and displacement correlations in imbibition. *J Colloid Interface Sci* **609**, 384–392 (2022).

72. Blunt, M., King, M. J. & Scher, H. Simulation and theory of two-phase flow in porous media. *Phys Rev A (Coll Park)* **46**, 7680–7699 (1992).

Corresponding author: Sharon Ellman, sharon.ellman@ugent.be

# Supporting information for

# "Validating mechanistic models of fluid displacement during imbibition"

*Sharon Ellman[1,2], Arjen Mascini[1,2] and Tom Bultreys[1,2]*

*[1]PProGRess,Dept. of Geology, Ghent University, Krijgslaan 281/ S8, 9000 Ghent, Belgium*

*[2]Centre for X-ray Tomography, Ghent University, Proeftuinstraat 86, 9000 Ghent, Belgium*

This document elaborates on the equations used to calculate the invasion-Pc values for snap-offs as described in Valvatne and Blunt[1] and cooperative pore-fillings as described in Ruspini et al.[2]. It also includes results obtained from pore network extraction B.

The following equations were used to calculate invasion-Pc for snap-offs:

- The invasion-Pc of snap-offs were calculated using the workflow put forward in Valvatne and Blunt[1], but with the corrections shown below, based on Bultreys et al. [3]

$$P_{c,1} = \frac{\sigma}{r} \cdot \frac{\cos(\theta_a + \beta_1)}{\cot\beta_1 + \cot\beta_3 - b_3 \cdot \sin\beta_1} \qquad \textit{Equation 1}$$

$$P_{c,2} = \frac{\sigma}{r} \cdot \frac{\cos\theta_a \cdot \cot\beta_1 - \sin\theta_a + \cos\theta_{h,2} \cdot \cot\beta_2 - \sin\theta_{h,2}}{\cot\beta_1 + \cot\beta_2} \qquad \textit{Equation 2}$$

$$P_c = \max(P_{c,1},\ P_{c,2}) \qquad \textit{Equation 3}$$

  Where $P_c$ is the snap-off pressure, σ is the interfacial tension, $r$ is the radius of the throat, $\theta_a$ is the advancing contact angle, $\beta_i$ is the half angle of throat-corner $i$ (with $\beta_1 \leq \beta_2 \leq \beta_3$), $\theta_{h,i}$ is the hinging contact angle in throat-corner $i$ and $b_i$ is the wetting layer thickness in throat-corner $i$. These equations arise from the assumption that the fluid-fluid interface which advances first is located in the sharpest corner. This interface then either meets the hinging interface in the corner with the largest angle (Equation 1), or the interface in the remaining corner which can be hinging or advancing (Equation 2).

- The cooperative pore-filling invasion Pc values were calculated using equations 16 to 23 in Ruspini et al.[2].

Corresponding author: Sharon Ellman, sharon.ellman@ugent.be

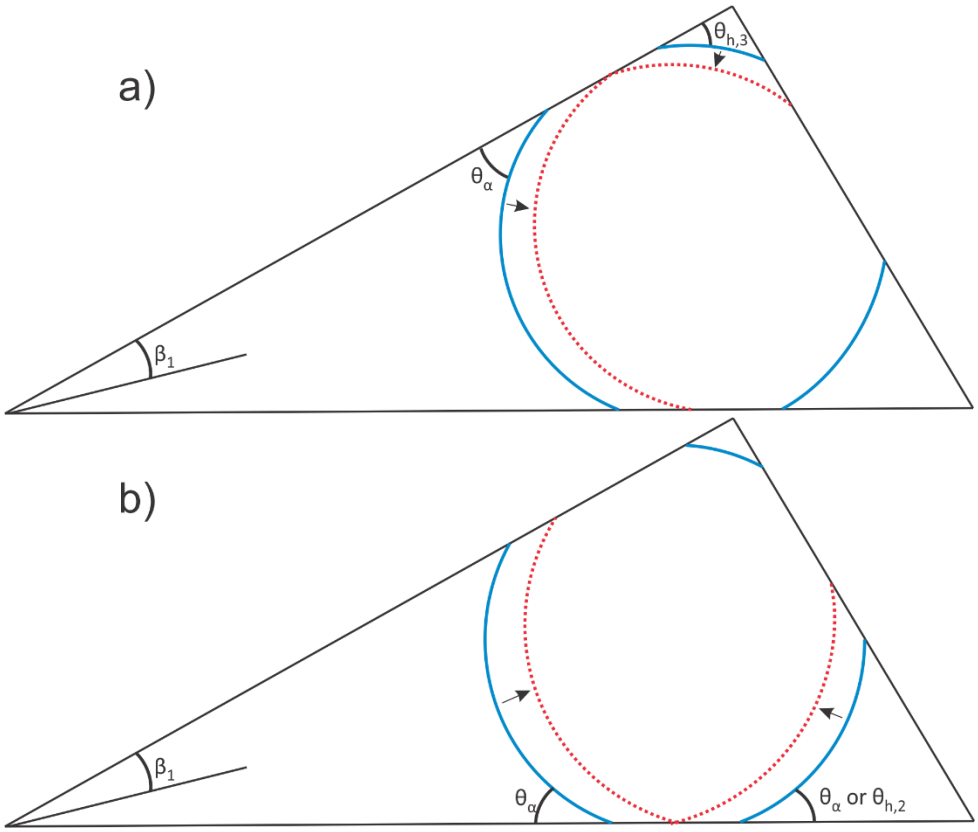


*Figure S 1: The meniscus (solid blue) is advancing forwards in the direction of the arrows. Snap-off occurs when the menisci from 2 corners touch. This position is shown in dotted red. a) The interfaces in the sharpest and most oblique corners advance. b) The interfaces in the sharpest and remaining corners advance. The scenarios are expressed by* **Equation 1** *and* **Equation 2** *respectively.*

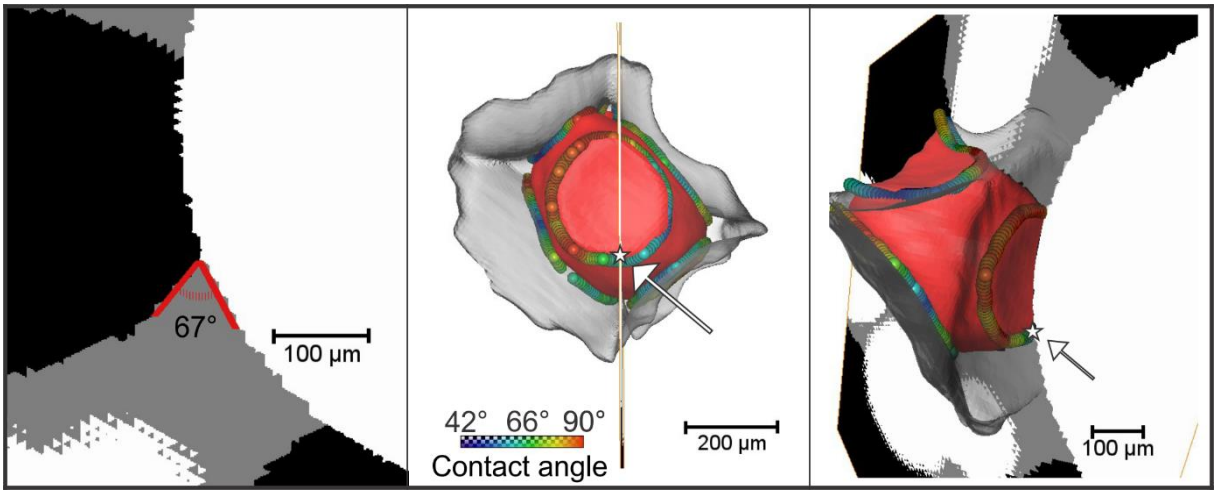


*Figure S 2: Manually measured geometric contact angle.*

Corresponding author: Sharon Ellman, sharon.ellman@ugent.be

*Table 4: invasion-Pc predicted for the remaining five piston-like displacements in pore network extraction A and their equivalent predicted invasion-Pc using pore network extraction B. In extraction B, three of these displacements were classified as piston-like displacements or cooperative pore-fillings that were one pore in size. The remaining two displacements included fillings of multiple pores in extraction B, hence their invasion-Pc could not be determined.*

| Pore network extraction A (Pa) | Pore network extraction B (Pa) |
|---|---|
| 234 | 185 |
| 218 | 86 |
| 292 | 232 |

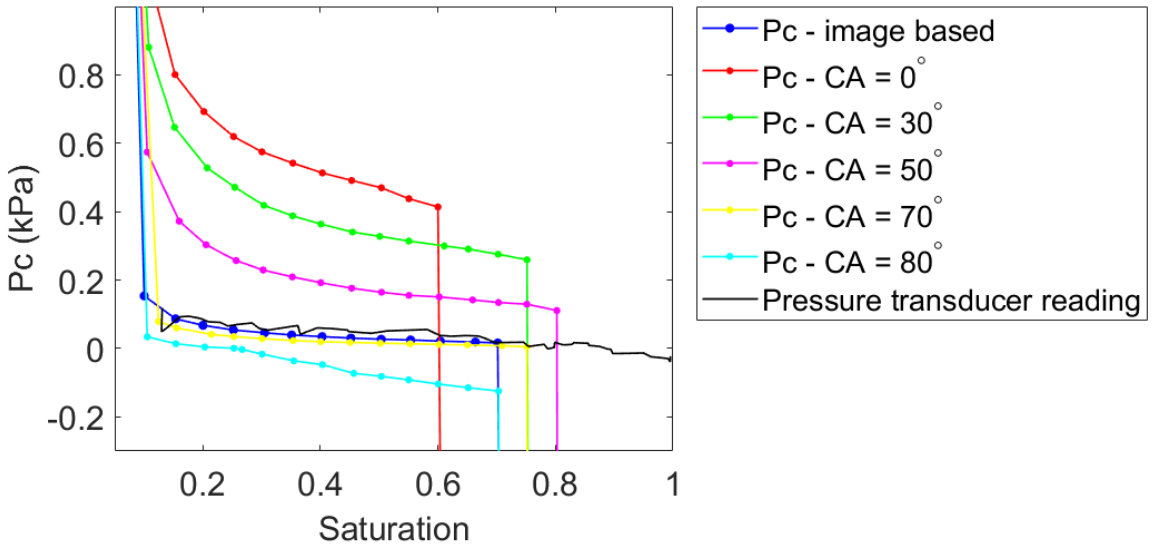


*Figure S 3: PNM simulations using several sets of contact angles. Using the local image-based contact angles yields a Pc-curve closest to the pressure transducer readings.*

*Table 5: The relative proportion of displacements simulated by the PNM categorised by type, for several sets of contact angles. This highlights the sensitivity of PNM to contact angle.*

| | Displacement type | | |
|---|---|---|---|
| **Contact angle** | **Snap-off (%)** | **Piston-like (%)** | **Cooperative (%)** |
| **0°** | 0 | 10 | 90 |
| **30°** | 0 | 26 | 74 |
| **50°** | 0.2 | 68.8 | 31 |
| **70°** | 28 | 70 | 2 |
| **80°** | 40 | 53 | 7 |

Corresponding author: Sharon Ellman, sharon.ellman@ugent.be

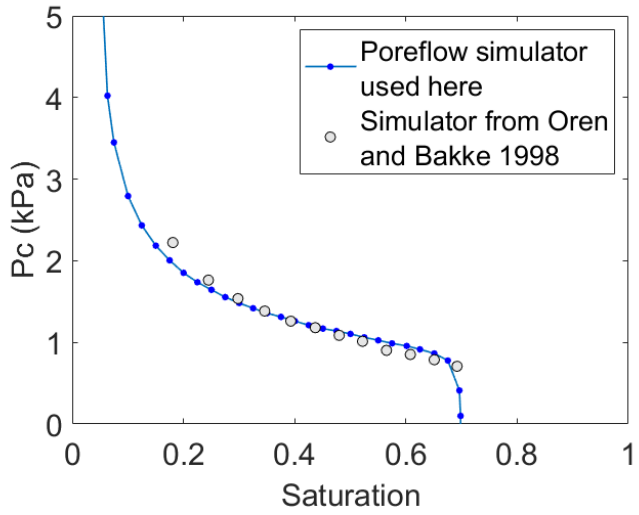


*Figure S 4: Imbibition simulation on an open-source Bentheimer sandstonde PNM (Gildehaus varietal) with the PNM extractor and simulator used in our manuscript, compared to the results by Oren and Bakke[4] (the grey dots are the same as those in the Figure from Patzek[5]).*

## Results obtained using pore network extraction B

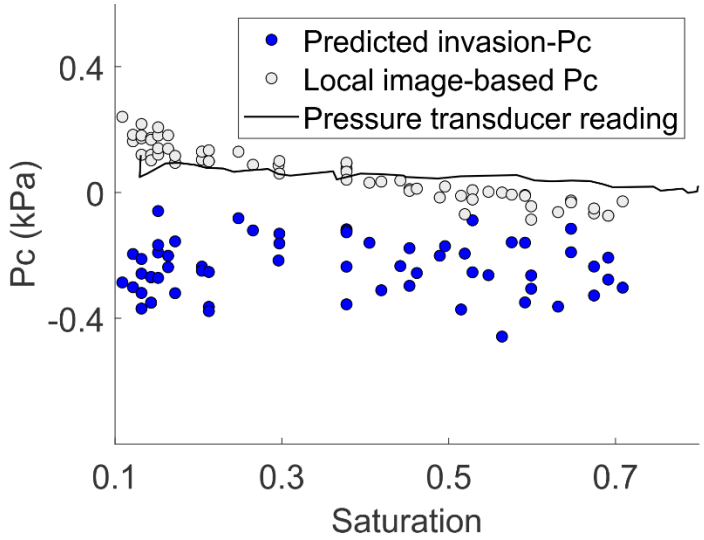


*Figure S 5: Predicted invasion-Pc for cooperative pore fillings plotted against saturation, compared with the local image-based Pc and the pressure transducer readings. The results are from pore network extraction B.*

Corresponding author: Sharon Ellman, sharon.ellman@ugent.be

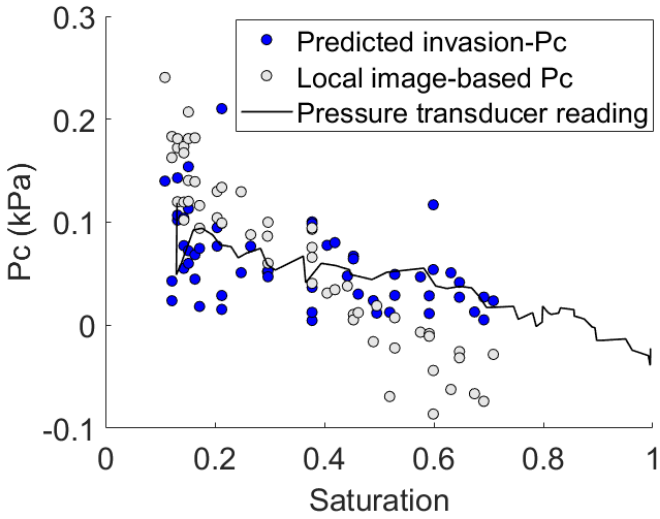


*Figure S 6: Predicted invasion-Pc of snap-offs simulated around pores assumed to be filled by cooperative pore-fillings. The results are from pore network extraction B.*

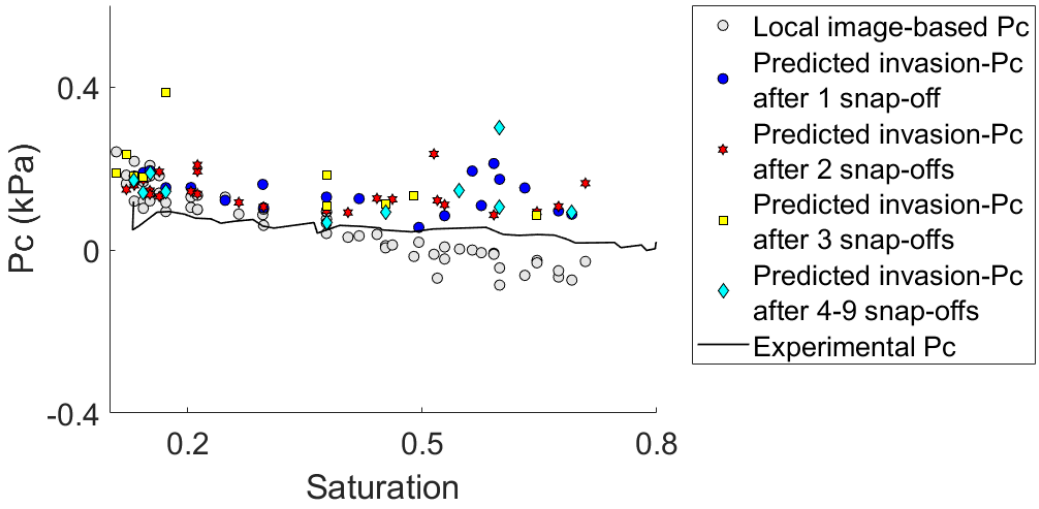


*Figure S 7: This graphs show the results after snap-offs were simulated. It shows predicted invasion-Pc for cooperative pore-fillings plotted against saturation, compared with the local image-based Pc and the pressure transducer readings. The results are from pore network extraction B.*

Corresponding author: Sharon Ellman, sharon.ellman@ugent.be

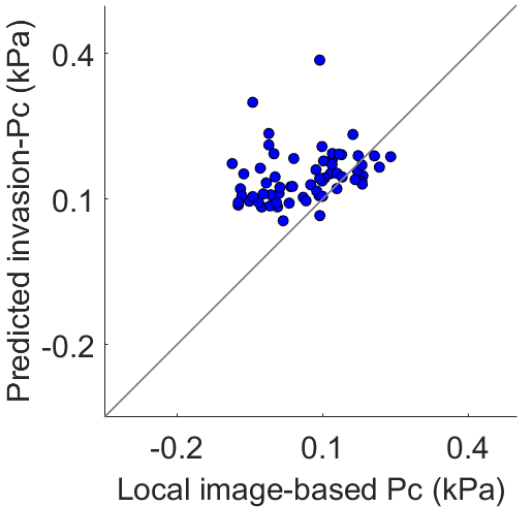


*Figure S 8: This graphs show the results after snap-offs were simulated. It shows predicted invasion-Pc for cooperative pore-fillings plotted against local image-based Pc. The results are from pore network extraction B.*

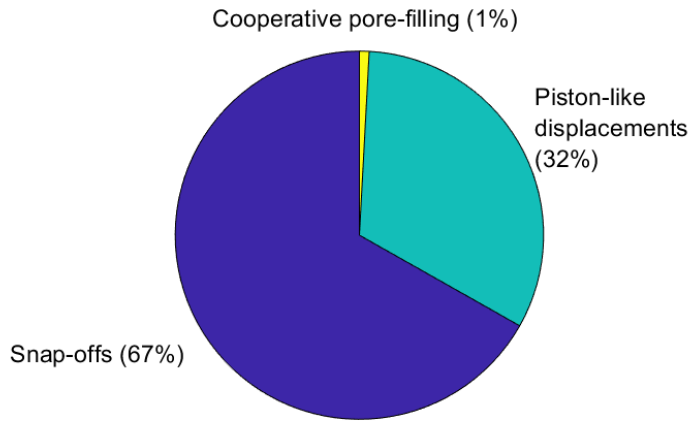


*Figure S 9: Proportions of the different types of displacements assuming the sequential filling approach is realistic. The original 78 single pore cooperative pore-fillings were thus found to be this combination of different displacement types (76 piston-like displacements, 2 cooperative pore fillings and 157 snap-offs). The results are from pore network extraction B.*

Corresponding author: Sharon Ellman, sharon.ellman@ugent.be

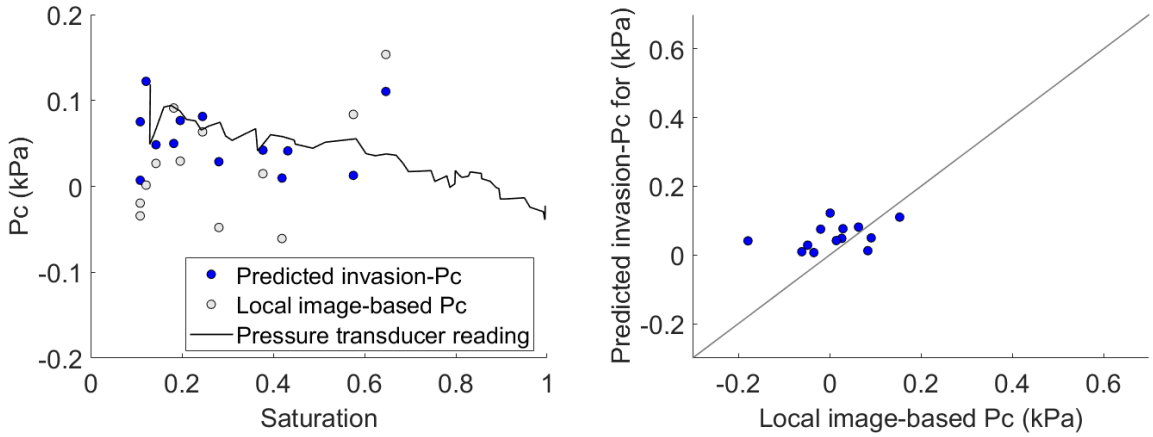


*Figure S 10: Left) Predicted invasion-Pc for snap-offs plotted against saturation, compared with the local image-based Pc and the pressure transducer readings. Right) Predicted invasion-Pc for snap-offs plotted against local image-based Pc. The results are from pore network extraction B.*

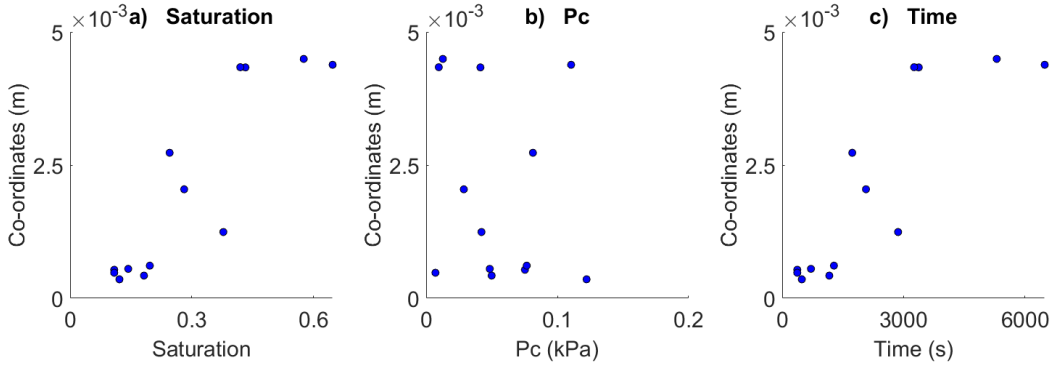


*Figure S 11: Saturation, predicted invasion-Pc and time plotted against distance from the inlet for each snap-off identified in the image analysis. The results are from pore network extraction B.*

Corresponding author: Sharon Ellman, sharon.ellman@ugent.be

## Predicted invasion-Pc values using set contact angles, instead of local geometric contact angles (a contact angle sensitivity study)

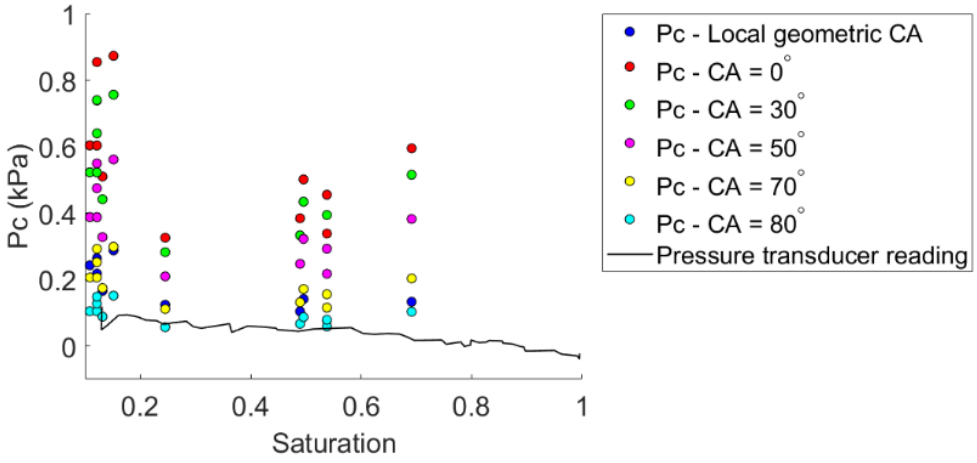


*Figure S 12: Predicted invasion-Pc values for piston like fillings, using different contact angles. The wise range in calculated Pc depending on the contact angle used, emphasizes the sensitivity to contact angle.*

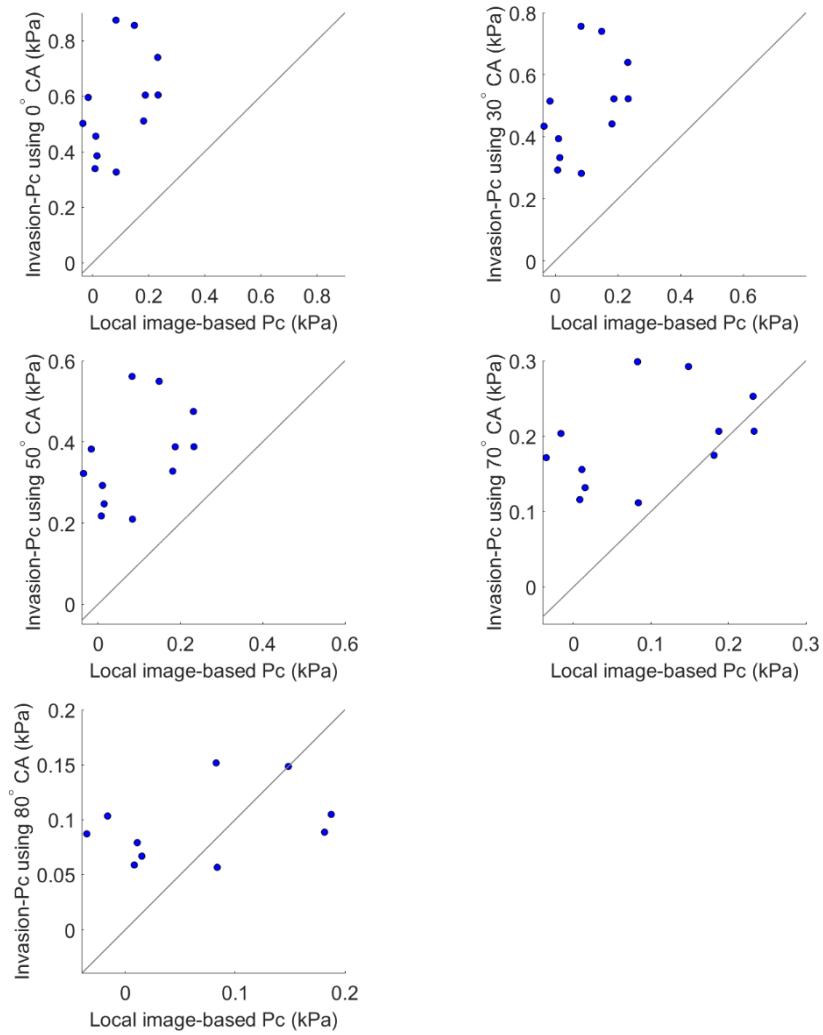


*Figure S 13: Predicted invasion-Pc values for piston like fillings, using different contact angles, plotted against local image-based Pc.*

Corresponding author: Sharon Ellman, sharon.ellman@ugent.be

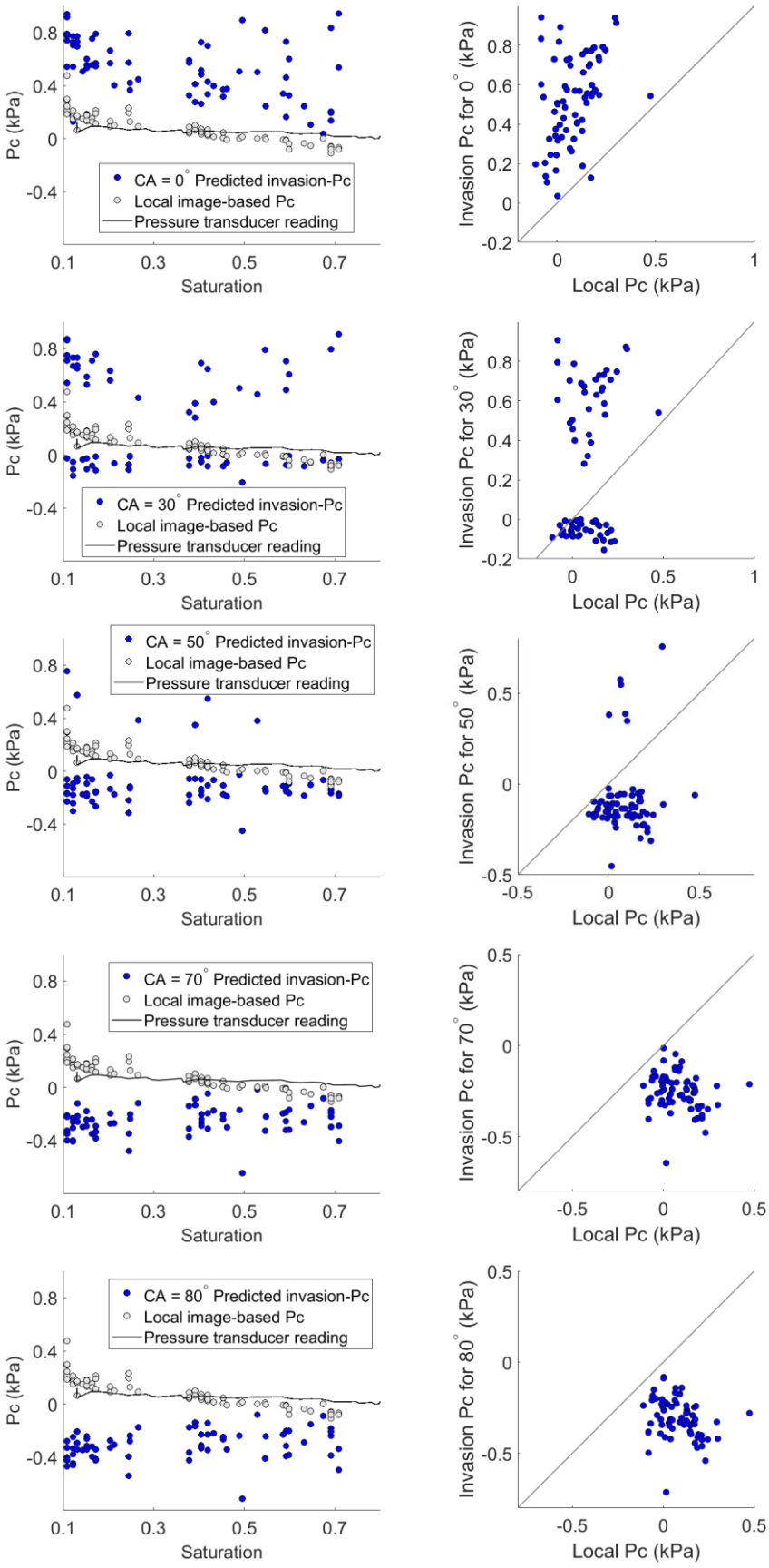


*Figure S 14: (Left) Predicted invasion-Pc values for cooperative pore fillings using different contact angles. (Right) Predicted invasion-Pc values for cooperative pore fillings using different contact angles plotted against local image-based Pc.*

Corresponding author: Sharon Ellman, sharon.ellman@ugent.be

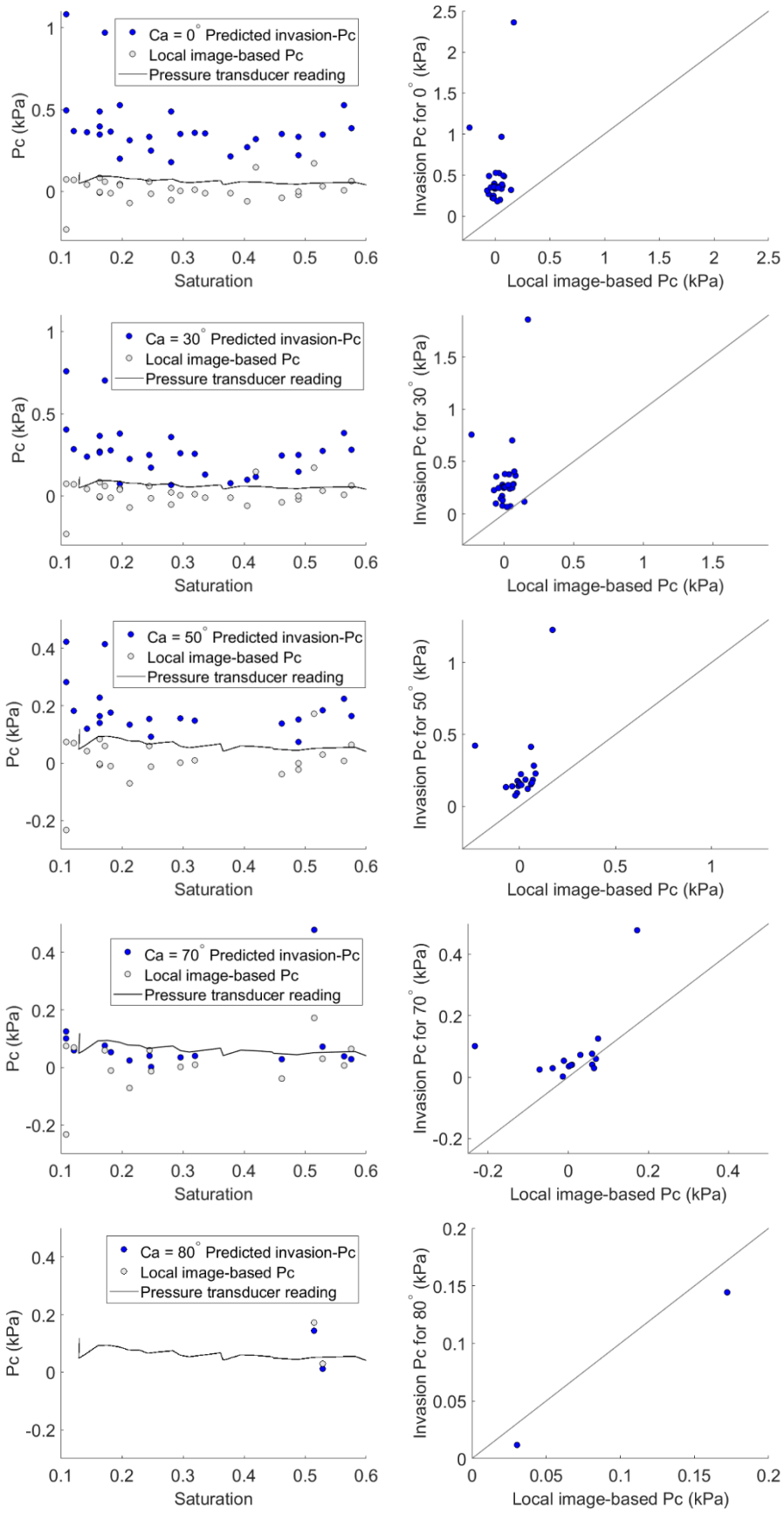


*Figure S 15: (Left) Predicted invasion-Pc values for snap-offs using different contact angles. It is worth noting that at lower contact angles, more of the snap-offs identified in the image analysis have Pc values which are calculable. (Right) Predicted invasion-Pc values for snap-offs using different contact angles plotted against local image-based Pc.*

Corresponding author: Sharon Ellman, sharon.ellman@ugent.be

## References


1. Valvatne, P. H. & Blunt, M. J. Predictive pore-scale modeling of two-phase flow in mixed wet media. *Water Resour Res* **40**, 1–21 (2004).

2. Ruspini, L. C., Farokhpoor, R. & Øren, P. E. Pore-scale modeling of capillary trapping in water-wet porous media: A new cooperative pore-body filling model. *Adv Water Resour* **108**, 1–14 (2017).

3. Bultreys, T., Singh, K., Raeini, A. Q., Ruspini, L. C., Øren, P.-E. P. E., Berg, S., Rücker, M., Bijeljic, B. & Blunt, M. J. Verifying Pore Network Models of Imbibition in Rocks Using Time-Resolved Synchrotron Imaging. *Water Resour Res* **56**, 1–23 (2020).

4. Øren, P. E., Bakke, S. & Arntzen, O. J. Extending Predictive Capabilities to Network Models. *SPE Journal* **3**, 324–335 (1998).

5. Patzek, T. W. Verification of a Complete Pore Network Simulator of Drainage and Imbibition. *SPE Journal* **6**, 144–156 (2001).


Corresponding author: Sharon Ellman, sharon.ellman@ugent.be